Noumea: A new multi-mission Cal/Val site for past and future altimetry missions?

Clémence Chupin[1], Valérie Ballu[1], Laurent Testut[1], Yann-Treden Tranchant[1], Jérôme Aucan[2]

[1]Littoral Environnement et Sociétés (LIENSs), UMR 7266, CNRS/La Rochelle Université, 2 rue Olympe de Gouges, 17000
5 La Rochelle, France : valerie.ballu@univ-lr.fr (V.B.), laurent.testut@univ-lr.fr (L.T.), yanntreden.tranchant1@univ-lr.fr (Y.-T.T.)

[2] Pacific Community Centre for Ocean Science, Nouméa, Nouvelle-Calédonie : jerome.aucan@ird.fr (J.A)

Correspondence to: Clémence Chupin (clemence.chup1@gmail.com)

Abstract. To better understand sea level evolution in coastal areas, one needs to link and combine global observations from
10 altimetry satellites with the scattered but long-term tide gauges measurements. In New-Caledonia, the Noumea lagoon is an example of this challenge as altimetry, coastal tide gauge and vertical land movements from Global Navigation Satellite Systems (GNSS) do not provide consistent information. The GEOCEAN-NC 2019 field campaign tries to address this question with the deployments of *in situ* instruments in the lagoon, with a particular interest for the crossing point of three different altimetry tracks (Jason/Sentinel-3a). Thanks to GNSS buoy and pressure gauge observations, we propose a method to virtually
15 transfer the Noumea tide gauge offshore, to obtain a long-term sea surface height (SSH) time series at the altimetry crossover point. We also reprocess the 20Hz along-track data from Jason and Sentinel-3a Geophysical Data Records (GDR) with the best correction parameters in the area. These two SSH time series (*i.e. in situ* and altimetry) allow us to compute the altimeter biases time series over the entire Jason and Sentinel-3a period. With our 3 weeks field campaign, we reanalyse about 20 years of altimetry observations and find inter-mission biases consistent with historical calibration sites, thus further increasing our
20 knowledge of the local sea level rise in this region. This offers many opportunities to develop Cal/Val activities in the lagoon, which is also the subject of several experiments for the scientific calibration phase of the future large swath altimetry mission SWOT.

Short summary. Altimetry satellites are essential to monitor and understand sea level evolution around the world with rare
25 accuracy of mm/year. But these systems must also be qualified and controlled, especially approaching the coast. Using long-term sea level time series from Noumea tide gauge (New-Caledonia) and *in situ* data collected during the GEOCEAN-NC campaign, we propose a method to re-analyse about twenty years of altimetry observations and re-address the question of sea level evolution in the lagoon.

1. Introduction

In the context of the global climate change, accurate monitoring of sea level in coastal zones is particularly needed. In these areas, the sea level and its evolution can be very different from the open ocean, due to a number of particularities as for example the presence of fresh water coming from estuaries, very shallow water depth, large tidal range or rapid morpho-dynamics

35   evolution. Since the 90s, altimetry satellites provide invaluable information about the open ocean circulation, waves, ice melting rates and global sea level variation around the world with centimetric accuracy for the surface height and mm/year accuracy for rates. Reaching this level of accuracy remains a real challenge and precise validation and calibration experiments (hereafter named Cal/Val activities) are thus required to characterize the performance of measurement systems and monitor their stability over time. Since the launch of the first altimetry mission, these operations enabled, for example, the detection of

40   significant drift in the TOPEX/Poseidon observations (Nerem et al., 1997) or problems in algorithms and instruments (e.g. the unaccounted-for bias for Jason 1 and 2 missions describe in Willis, 2011).

To achieve the centimetric level, absolute Cal/Val experiments require the use of the most accurate altimetry data, with the best orbit and instrumental parameters and the up-to-date geophysical corrections. It also involves overcoming the limits of *in*

45   *situ* measurement systems, with the deployment over long periods of reliable and accurate instruments that can be linked to the same global reference frame as the satellite data. The location of a Cal/Val site is also important: ideally, it should be close enough to the coast to have access to long-term tide gauge measurements and terrestrial observation systems (e.g. permanent GNSS, weather stations, etc.), but far enough to keep reliable altimetry data. In fact, altimetric measurements face important issues when approaching the coast, particularly because of land contamination of the altimeter and radiometer signals

50   (Gommenginger et al., 2011). Several dedicated sites around the world are used to monitor the evolution of the altimetry missions: Harvest in the USA (Haines et al., 2020a), Bass-Strait in Australia (Watson et al., 2011), Corsica in France (Bonnefond et al., 2019) and more recently Gavdos in Greece (Mertikas et al., 2018). Other regional specific studies also use Cal/Val methodology for different purpose and context such as for lake surface level (Crétaux et al., 2013), tropical area (Babu et al., 2015) or seafloor geodesy (Ballu et al., 2013). Varying methods and study area is important to have representative

55   estimation of altimeter biases (Bonnefond et al., 2011). For example, diversifying *in situ* instrumentation allow to reduce biases related to the technic used, and develop new sites help to avoid geographically correlated error, such as those due to a particular hydrodynamic configuration.

In line with these efforts to develop new Cal/Val sites and innovative method, our study focuses on the Noumea lagoon in

60   New Caledonia. At the interface between the open ocean and the coast, the lagoon is covered by several satellite tracks, and the Noumea tide gauge site provides a long-term sea level time series. Its unique location and the proximity to a national oceanographic research institute make it also a relevant site to test and improve *in situ* measurements techniques in the specific environment of a lagoon: this was done during the dedicated GEOCEAN-NC cruise in October 2019. Thanks to the variety of

observation collected as part of this field campaign, the present paper details a methodology to compare altimetry and *in situ*

65 measurements, following standards made for dedicated Cal/Val studies. Section 2 describes our study site and presents the GEOCEAN-NC cruise and its objectives. Section 3 is dedicated to the processing of the *in situ* data to reconstruct a long sea level time series under the altimetry tracks. Finally, section 4 details the reprocessing of the altimeter data, and concludes with the comparison with *in situ* observations.

2. Noumea study site

70 **2.1 The Noumea lagoon**

In the Southwest Pacific, the lagoon surrounding New Caledonia (Fig. 1a) is the world largest lagoon with a surface of 24,000 square kilometres. This lagoon is covered by many altimetry tracks from past and current nadir altimetry missions (TP/Jason, Sentinel-3a…) and is already the target of dedicated Cal/Val campaigns planned during the fast-sampling phase of the future SWOT large-swath mission (e.g. project "SWOT in the Tropics" - Gourdeau et al., 2020). A network of *in situ* measurements

75 has also been developed in New Caledonia, which includes tide gauges and permanent GNSS stations from the BANIAN network (Fig. 1a, resp. green and blue dots). The lagoon is also the subject of numerous geological, environmental and societal studies supported by the presence of IRD (Institut de Recherche pour le Développement) in Noumea, that offers expertise and resources to organize observation campaigns and analyses.

80 In the present study, we particularly focused on the southern part of the lagoon, near Noumea city (hereafter named "Noumea lagoon", Fig. 1b). With an average depth of 15-20 m, its dynamics are mainly dominated by semi-diurnal tides with a mean tidal range varying from about 1.4 m at spring tides to 0.6 m at neap tides (Douillet, 1998). A notable interest of this area is the intersection of three altimetric tracks (Fig. 1b, black lines) at about 13 km from the main land coast and 28 km from Numbo tide gauge: the TP/Jason pass #162 and Sentinel-3a passes #359 and #458.

85 **2.2 The GEOCEAN-NC 2019 field campaign**

In October 2019, the GEOCEAN-NC oceanographic cruise was organised in Noumea lagoon on the R/V Alis (Ballu, 2019) to address the question of long-term sea level evolution in this area. This question remains an unresolved issue because altimetry, tide gauge and GNSS land-based observations do not provide consistent information (Aucan et al., 2017; Martínez-Asensio et al., 2019; Ballu et al., 2019).

90

For that, one objective was to collect *in situ* data under satellite tracks. For the 3 weeks of the campaign, the coastal version of the CalNaGeo GNSS carpet was towed by R/V ALIS along and across altimetry tracks, and inside and outside the lagoon (Fig. 1b, blue lines). Several studies have demonstrated the capability of CalNaGeo to accurately the map sea surface in motion in various sea and weather conditions (Chupin et al., 2020; Bonnefond et al., 2022). A GNSS buoy was also moored at multiple
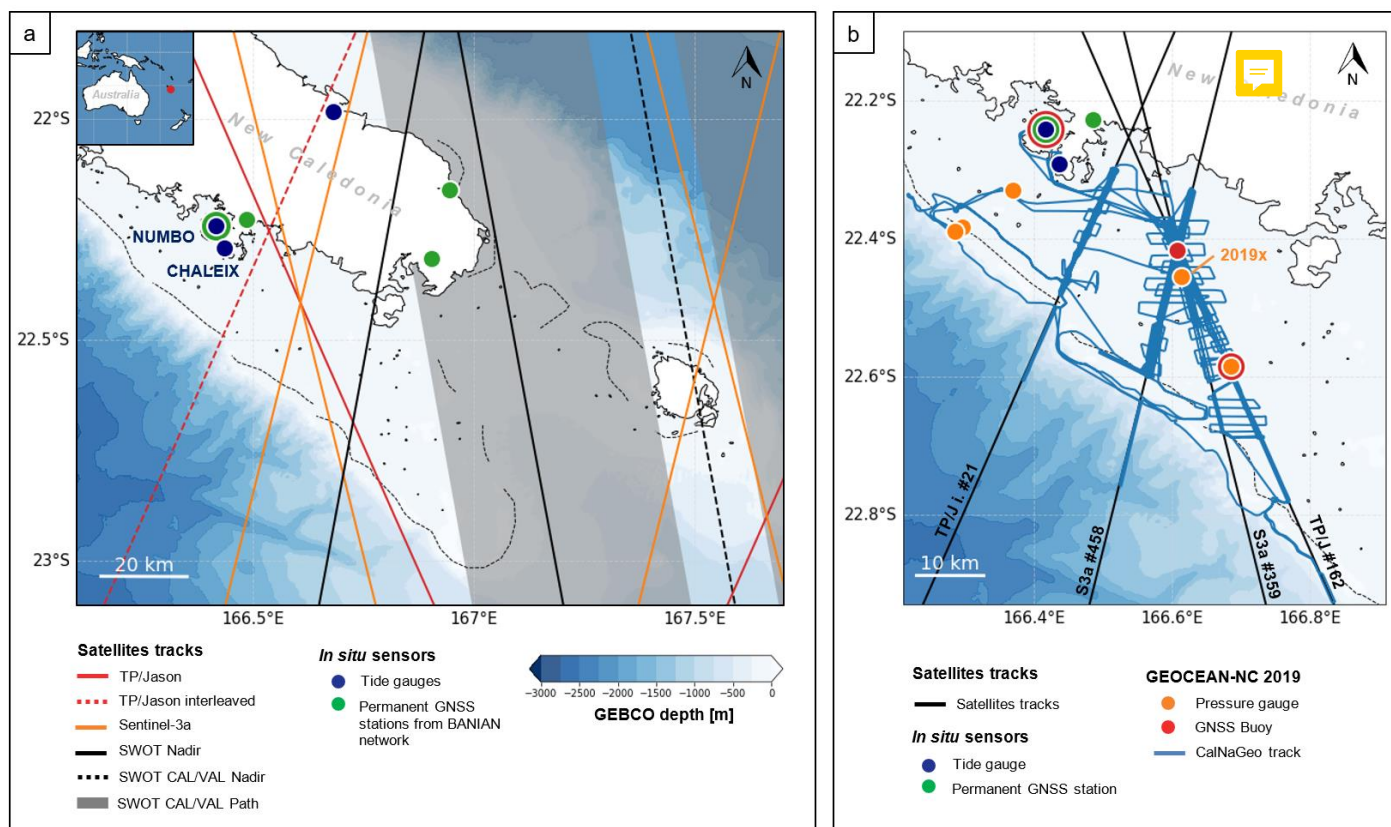
Figure 1. (a) Map of the Noumea lagoon in the South Pacific Ocean and localisation of the main altimetry tracks and *in situ* sensors. The bathymetry from the GEBCO global model (GEBCO Compilation Group 2020) is represented by a blue gradient and the dotted lines represent the coral reefs. (b) Location of the sensors used (tide gauge, GNSS stations) and deployed (pressure gauge, GNSS buoy and CalNaGeo GNSS carpet) during the GEOCEAN-NC 2019 cruise. Note that some sensors were deployed at the same location: the coloured dots representing them therefore overlap.

95   location in the lagoon (Fig. 1b, red dots). Developed by DT-INSU, it consists of a GNSS antenna (Trimble Zephyr 3) supported by a floating structure, with a metal cylinder containing the receiver (Trimble NetR9) and batteries (see picture in Fig. 3). GNSS buoys are commonly used for Cal/Val activities (Born et al., 1994; Watson et al., 2011; Bonnefond et al., 2013) and many studies have demonstrated their capability to provide sea level records with centimetric accuracy (André et al., 2013; Gobron et al., 2019). During the campaign, a calibration session at the Noumea Numbo tide gauge was performed to assess

100   the performance of these GNSS instruments. Our results show that, despite vertical biases (-1.7 ± 0.5 cm for the buoy and -0.6 ± 0.4 cm for CalNaGeo) that could result from terrestrial geodesy measurements uncertainties and GNSS processes, these two instruments are consistent with the radar gauge observations (more details in Chupin et al., 2020).

During the mission, five pressure sensors (Seabird SBE26plus) were moored in the lagoon at depths ranging from 12 to 20 m

105   (Fig. 1b, orange dots). All sensors recorded pressure variations at the seafloor between October 2019 and November 2020.

Three of them were installed along a profile linking the Noumea tide gauge and the outside border of the coral reef, with the aim of quantifying the setup induced by wind and waves. Two other gauges were deployed along the TP/Jason altimetry track #162 for altimetry analysis purpose. A calibration phase a hyperbaric chamber before and after their deployment was conducted to check the proper functioning and overall drift of the gauges (detailed results are available in Appendix A).

110

Taking advantage of all observations acquired as part of the GEOCEAN-NC cruise, we thus develop a method to reconstruct a long term virtual *in situ* sea level time series at the altimetry crossover point.

3. Reconstruction of a long term virtual *in situ* sea level time series under the altimetry tracks

3.1 Method

115 The objective of our analyse is to compare the offshore altimetry measurements at the Jason/Sentinel-3a crossover with *in situ* observations. For that, two methods can be adopted (Bonnefond et al., 2011): an indirect comparison, where the *in situ* measurement is distant from the altimetry pass (typically a coastal tide gauge), and a direct comparison where *in situ* sea surface height (SSH) is directly observed at the comparison point with instrumented platforms (as in Harvest Cal/Val site) or precise GNSS buoys. Following the method of Watson et al. 2011, we developed a mixed approach using both *in situ*
120 measurements from the GEOCEAN-NC campaign and the Noumea tide gauge records.

Figure 2 summarises the three steps of this method, that are detailed in the following sections:

Step 1. The GNSS buoy deployed at the altimetry crossover point during the GEOCEAN-NC cruise provides SSH in the same reference system as the altimetry measurements.

125 Step 2. To extend the comparison, we use measurements from the pressure sensor closest to the altimetry crossover (hereafter named *2019x* pressure sensor). By computing the mean offset between the GNSS buoy and this pressure gauge on common observation periods, the 2019x pressure sensor observations are linked to a global reference frame and virtually transferred to the altimeter comparison point.

Step 3. Finally, the SSH time series from Noumea tide gauge site is used to increase the comparison duration. Using its
130 common year of observation with the 2019x pressure gauge, the tide gauge is virtually transferred to the crossover location by computing a tidal and datum correction.
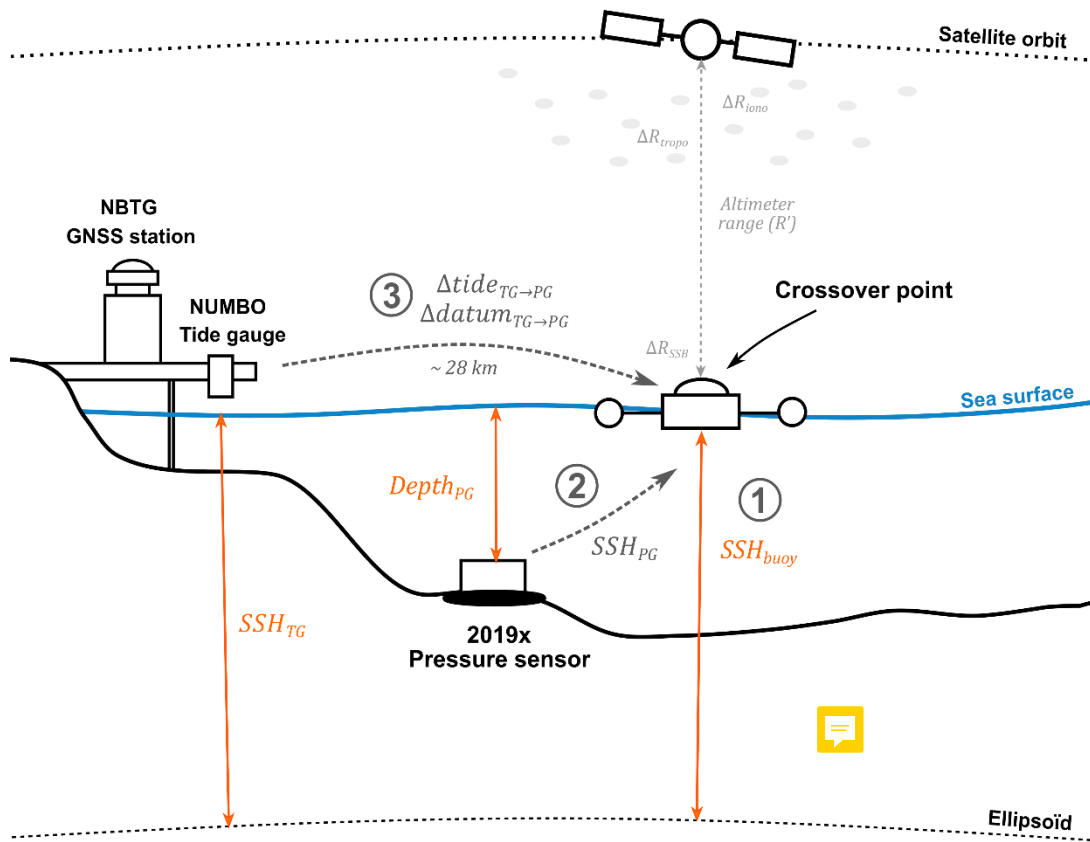
Figure 2. Configuration of the sensor's deployment. They are used to derive a long term *in situ* sea level time series under the altimetry tracks. The three steps of the methodology are represented by the circled numbers.

3.2 GNSS Buoy sea level measurements

The first step of the data analysis concerns the buoy measurements at the altimeter crossover point (Step 1 in Fig. 2). The
135   kinematic processing of the GNSS data was carried out with the GINS software in Precise Point Positioning (PPP) mode (Marty et al., 2011). Developed in the 90s, this method makes it possible to determine a point position without using a reference GNSS base (Zumberge et al., 1997), and recent improvements of GNSS processing allows to compute the height of a GNSS buoy with a centimetric accuracy (Fund et al., 2013). The buoy observations are processed with GINS PPP mode with the integer ambiguity resolution option (details of the processing option in Appendix B, Table B1).

140

The resulting sea level time series, expressed with respect to the GINS internal reference system, is linked to the IAG-GRS80 ellipsoid by applying a time-dependant vertical sca. The distance from the GNSS Antenna Reference Point (ARP) to sea

level, determined during stati ssions, is also subtracted. After a first data selection to keep positions determined with more than 10 satellites and remove outliers, the resulting heights are filtered using a Vondrak filter with a 30 min cut-off frequency

145 (Vondrak, 1977) (Fig. 3). This filtering lead to a SSH time series cleaned from high frequency signal (short waves, …) (Step 1 in Fig. 2), adequate for a comparison with a 20 m depth bottom pressure records (Step 2 in Fig. 2).

During the buoy deployment, the area was overflown by the Sentinel-3a satellite on its track #359, which allows a direct comparison with the buoy measurements. At the time of the overfly, the SSH difference between the filtered buoy time series

150 and altimetry measurements is about 1.7 cm (Fig. 3). As this single comparison remains limited we then use the 1-year pressure sensor observations to extend the time series of *in situ* measurements.
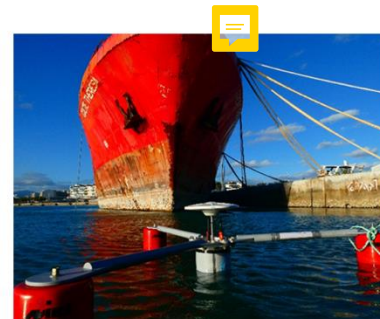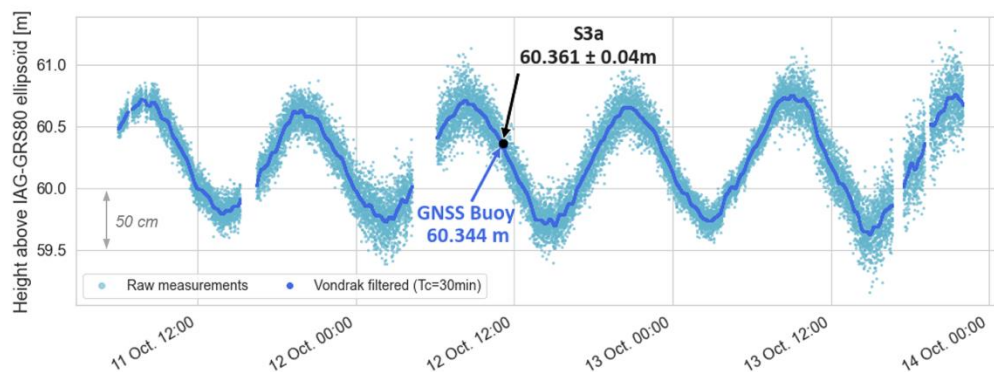
Buoy deployment in the Noumea harbor

Figure 3. GNSS Buoy raw (light blue) and Vondrak filtered (dark blue) sea level heights above the IAG-GRS80 ellipsoid.

3.3 Pressure sensor observations

To extend the comparison, we used the pressure gauge 2019x, located at about 4 km south of the Sentinel-3a and Jason ground tracks crossing point (Fig. 1b, orange dot). The pressure gauge deployment site was chosen as a compromise between distance

155 to the tracks intersection and the depth limitation of the SBE26plus (20 m). Despite of the distance, we assume that the 2019x gauge roughly monitor the same sea as the GNSS buoy. This assumption is encouraged by the high correlation between their Significant Wave Height (SWH) observations (details of this analysis are shown in Appendix C).

Consequently, we used the GNSS buoy observations to tie the pressure gauge measurements into a reference frame similar to

160 the altimetry data (Step 2 in Fig. 2). The 2019x seafloor pressure is converted to equivalent hydrostatic heights, using atmospheric pressure time series from ERA5, the latest climate reanalysis produced by ECMWF (Hersbach et al., 2018), at the pressure gauge location, and the water column density computed with the pressure gauge temperature and a mean salinity value of 35.5 psu. The calibration phase of the 2019x sensor shows a linear trend of about -70 mm/year (more details in Appendix A), which is removed to obtain the final sea level time series from the 2019x pressure sensor.

165

The pressure gauge data are then tie to the ellipsoid by differencing the filtered GNSS buoy heights (Fig. 4a, dark blue) from the pressure sensor measurements (Fig. 4a, grey line). Over the 6-h of common observation period, the average difference is equal to 40.125 ± 0.030 m (Fig. 3b). Added to the hydrostatic heights of the pressure sensor, this offset allows us to obtain a 1-year sea level record at the intersection of the altimeter tracks, thereafter named SSH_{PG} (Step 2 in Fig. 2). However, to have

170   a longer *in situ* time series, we also considered the Noumea tide gauge dataset (Step 3 in Fig. 2).
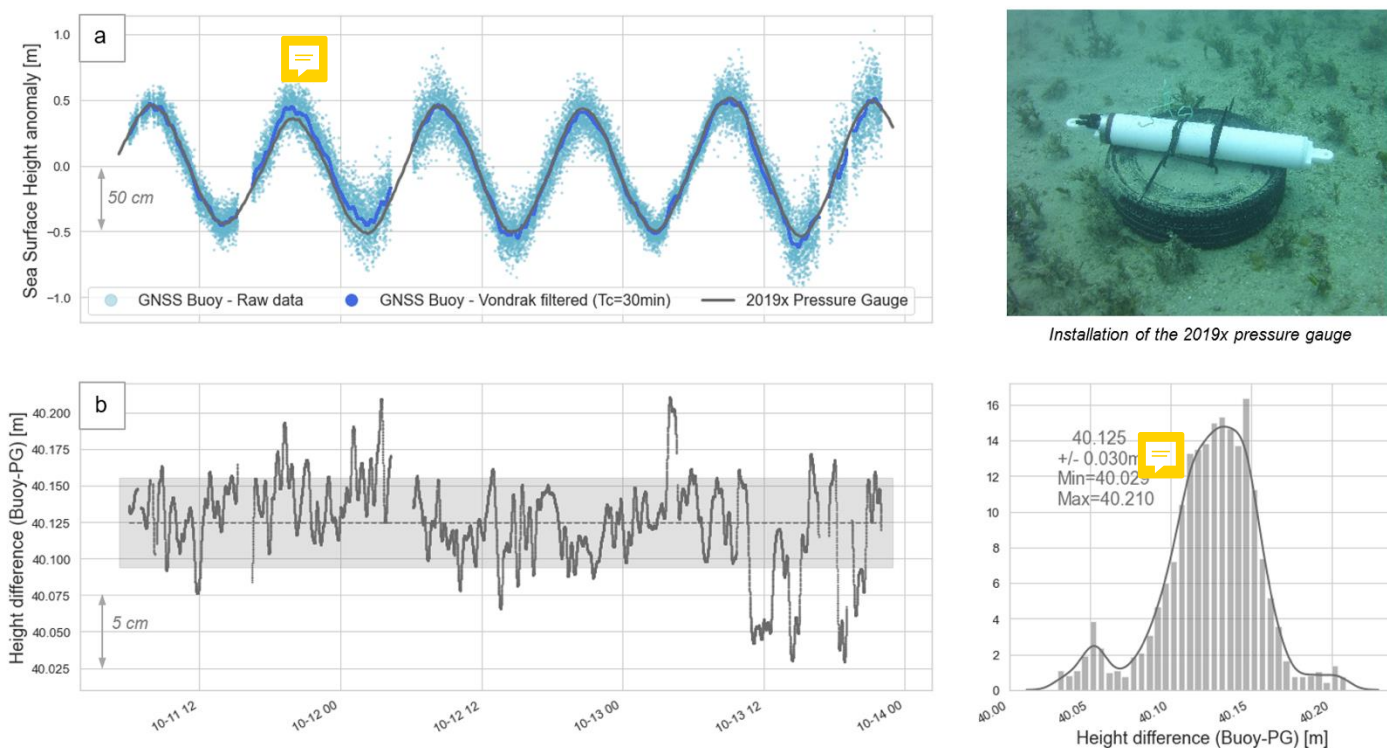
Figure 4. Comparison between GNSS buoy and 2019x pressure gauge observations / (a) Sea surface height anomaly from GNSS buoy raw data (light blue), GNSS buoy filtered data (dark blue) and 2019x pressure sensor (grey) / (b) Difference between filtered GNSS buoy and 2019x pressure gauge heights. The grey dotted line represents the mean difference (40.125 m), and the grey area represents the ± 1 standard deviation (3 cm). These differences are also showed on the lower right histogram.

3.4 Noumea tide gauge long term measurements

The French Hydrographic Service (Shom) provides sea level observations at Noumea through the Chaleix (operating from 1957-2005) and Numbo (2005 to present) tide gauges (Fig. 1a, blue dots). Before 1967, measurements were paper records, and electronic observations began in 1967. Thanks to a 6 months overlap of data collection, the old Chaleix site has been

175   linked to the new Numbo site, located about 6 km away (Fig. 1a, blue dots). Aucan et al., 2017 were thus able to reconstruct the whole time series by concatenating data from 1957 to 2018, making it one of the longest series available in the South

Pacific. In this paper, we used the data available online (http://uhslc.soest.hawaii.edu/data/ - ID 019) and regularly updated with the latest measurements from Numbo tide gauge. This 1-hour sampling sea level time series will be referred to as SSH_{TG} in the following, and covers the entire altimetry period and our study ([1967-2021]).

180

The Noumea tide gauge site and the altimeter crossover point are separated by about 28 km. The last step of our methodology is to bring tide gauge observations at the comparison point (Step 3 in Fig.2). For that, we consider the height residuals between 2019x pressure sensor and Noumea tide gauge measurements and compute a tidal and datum correction, as made by Watson et al. (2011) at the Bass Strait Cal/Val site. After linearly interpolating the 10 min pressure gauge data on the 1-hour tide gauge

185   time series over their common measurement period (Fig. 5a), we compute the difference $[SSH_{PG} - SSH_{TG}]$ (Fig. 5b – black). We then computed an harmonic analysis on these residuals to get the tidal gradient correction in amplitude and phase ($\Delta tide_{TG \to PG}$) and the datum correction ($\Delta datum_{TG \to PG}$) to apply on the tide gauge record. Tidal residuals are mainly due to semi-diurnal waves, with a contribution from M2, S2 and N2 of about 3.5 cm, 1.5 cm and 1 cm respectively. The resulting datum correction is estimated to be -56.2 cm, which is coherent at the order of a few centimetres with gradients from two

190   global gravity field models in the area (see Table E1 in Appendix E). After applying the tidal gradient and the datum offset, the difference $[SSH_{PG} - SSH_{TG}]$ have a Root-Mean-Square Error (RMSE) of 1.34 cm (Fig. 5b – grey), to compare with the 3.26 cm without these corrections.

Finally, we obtain an hourly *in situ* sea level time series at the altimeter comparison point (thereafter named $SSH_{in-situ}$) by

195   virtually transferring the Noumea tide gauge observations (Step 3 in Fig.2) :

$$SSH_{in-situ} = SSH_{TG} + \Delta tide_{TG \to PG} + \Delta datum_{TG \to PG} \qquad (1)$$

However, the altimeter fly over the area for about 10 seconds between 1 and 3 times per month (resp. for Sentinel-3a and Jason missions), and doing a simple linear interpolation of the hourly $SSH_{in-situ}$ at the satellite overfly time (t_{sat}) is not sufficient

200   to reproduce all the oceanic variability. We thus expressed the SSH_{TG} as a tide reconstruction at the time of the satellite flyby $- TGtide_{rec}(t_{sat}) -$ and add tide residuals linearly interpolated at the flyby time $- TGtide_{res}(t_{sat})$. Thus, for the final comparison with altimetry data, the $SSH_{in-situ}$ from Eq. (1) could be explained as:

$$SSH_{in-situ}(t_{sat}) = TGtide_{rec}(t_{sat}) + TGtide_{res}(t_{sat}) + \Delta tide_{TG \to PG}(t_{sat}) + \Delta datum_{TG \to PG} \qquad (2)$$

205   With this method, there are still inaccuracies in the determination of the sea level due to weather and local conditions, but the tide evolution is well considered.
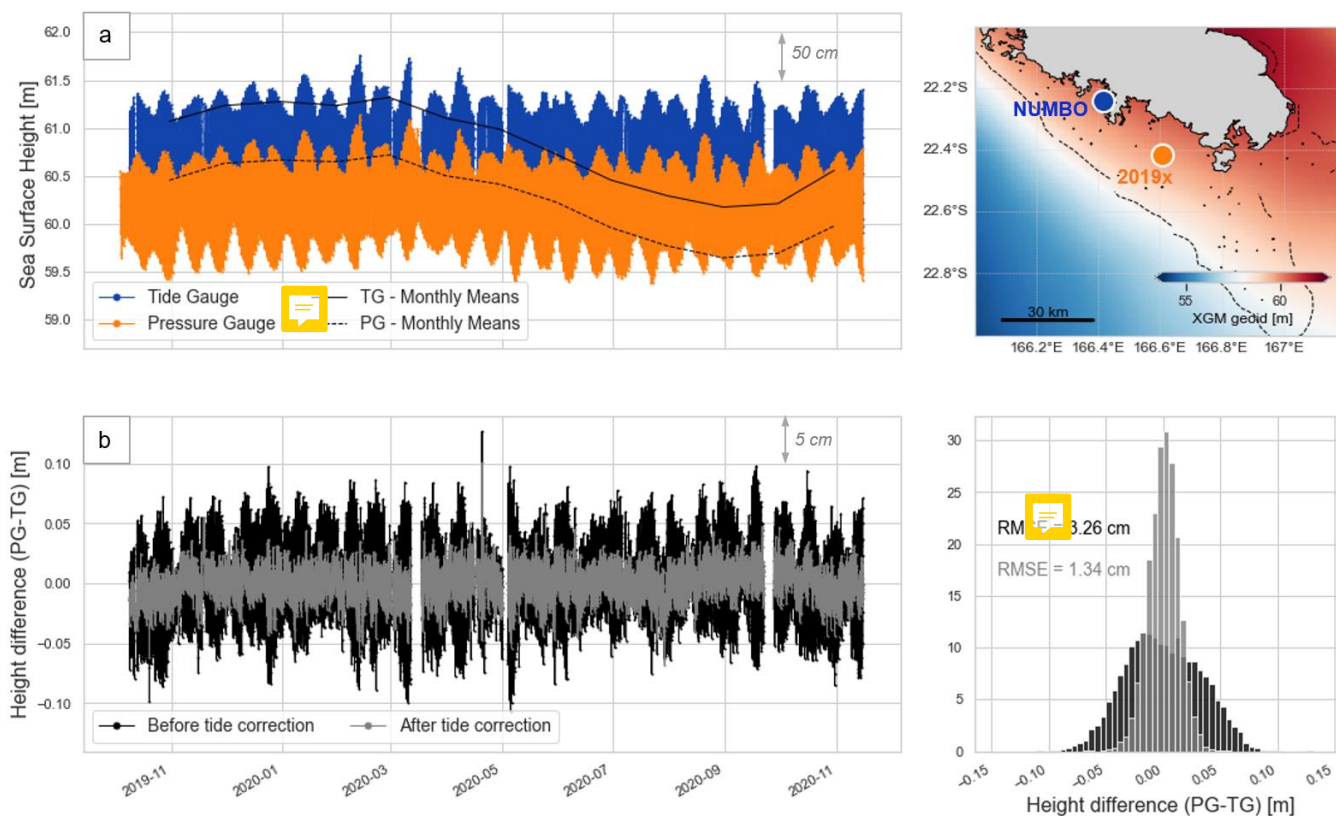
Figure 5. Tidal difference between the Noumea tide gauge (TG) and the 2019x pressure gauge (PG) / (a) Sea level record at 2019x pressure gauge (orange) and Numbo tide gauge (blue) during the common observation period (13 months). Monthly means are displayed in black (solid line for tide gauge, dotted line for pressure gauge). The two sensors are separated by about 28km. / (b) Height difference between PG and TG before (black) and after (grey) applying the tidal correction. These differences are also displayed on the histogram, with Root Mean Square Error (RMSE) values for both solutions.

4. Calibration/Validation of altimetry measurements

4.1 Altimetry data processing

210 **4.1.1 Jason and Sentinel-3a Geophysical Data Records (GDR)**

There is a large diversity of altimetry products and sources. In order to have homogeneous data, we tried to use the most recent data with the same format over the whole comparison period. For the Jason track #162, we use the last Geophysical Data Records (GDR) delivered by the AVISO+ FTP, that integrate precise orbits and up-to-date corrections for 20 Hz measurements (Table 2). For Sentinel-3a dataset, the SRAL Level 2 Marine data were used to ensure a global coverage of the lagoon. These

215 data are available on the EUMETSAT portals (until September 2022). From 2016 to 2019, the Sentinel-3a data were reprocessed using up-to-date standards of the Baseline Collection 004, used for Sentinel-3a products after 2019 (Table 1).

Table 1. Altimeter products used in the study

Mission	Jason			Sentinel-3a	
	Jason 1	Jason 2	Jason 3		
Cycles	1-259	1-303	1 - 219	3-52	53-81
Products	GDR-E	GDR-D	GDR-F	SR_2_WAT Baseline Collection 004	
				Reprocessed BP 2.61	Non-reprocessed BP 2.61/2.68
Source	AVISO+ FTP : https://www.aviso.altimetry.fr/en/home.html			EUMETSAT portals CODA : https://coda.eumetsat.int/#/home CODA REP : https://codarep.eumetsat.int/#/home	

4.1.2 Altimetric corrections used to derive sea level heights

220 During its propagation, the altimetric signal is delayed by multiple phenomena that must be consider to estimate the altimetric sea surface height (SSH_{alt}) with a centimetric accuracy. Thus, the altimeter range must be corrected for instrumental errors (R'), sea state biases (ΔR_{SSB}) and atmospheric delays (ΔR_{iono} and ΔR_{tropo}). The final objective of our study is to compare this SSH_{alt} with tide gauge observations, that contain the ocean tide signal and variations due to atmospheric dynamics. To have comparable values, it is therefore necessary to integrates geophysical corrections in the altimetric processing (ΔR_{geo}) to

225 account for the effect of ocean tide loading, pole and solid earth tides.

One of the major limitations of the coastal altimetry data is the quality of these atmospheric and geophysical corrections. By using the 20 Hz along-track products, we are thus able to select the most appropriate correction parameters or replace them by external products. In the GDR used for this study, the range is already corrected from instrumental errors (R'). We consider

230 the ΔR_{SSB} and the ΔR_{geo} parameters at 1 Hz from the GDR, that are linearly interpolated at the 20 Hz measurements.

Regarding the ionospheric correction (ΔR_{iono}), GDR files provide a correction based on the difference between the two altimeter frequencies that are sometimes very noisy. To have a better correction without degrading the altimeter observations, one way is to smooth this ionospheric correction over a 150 km profile (Imel, 1994). Following methods developed on other

235 historical Cal/Val sites (e.g. Watson et al., 2011), we use the mean ionospheric delay in the area between -23.85° and -22.5°, which covers part of the lagoon, the reef and the open ocean, and roughly corresponds to the recommended distance of 150 km.

The tropospheric delay (ΔR_{tropo}) can be divided into a wet and a dry component. About 90% of this delay is related to the dry

240 component, that can be estimated with atmospheric models (Chelton et al., 2001). We use the 1 Hz hydrostatic tropospheric correction provided in the GDR files, linearly interpolated at the 20 Hz measurements. The wet component of the troposphere

is related to the water vapor content in the atmosphere, that is variable in time and space, particularly when approaching the coast. Onboard radiometers can estimate these variations along the track, but due to their larger footprint, they are contaminated by land before the altimeter measurements. In the lagoon, the effect of the land contamination is visible when approaching the

245   main island, but at our comparison point, the radiometer correction seems to be exploitable for both Jason and Sentinel-3a missions (more details in Appendix D). To confirm this hypothesis, we also test to other datasets: (1) a wet tropospheric delay provided by the European Center for Medium Range Weather Forecasting (ECMWF) and (2) a wet tropospheric correction computed from inland permanent GNSS stations (more details about this processing in Appendix D). When comparing with the *in situ* observations, we will be able to analyse the impact of these different solutions.

250

Finally, altimetry satellites do not fly over the exact same point at each pass: it is therefore necessary to consider the height difference between the comparison point and the actual pass of the satellite track, which we approximate to the geoid height difference between the 2 points ($\Delta R_{geoïd}$). Using CalNaGeo observations during the GEOCEAN-NC campaign (Fig. 1b, blue lines), we have shown that the XGM 2019e gravity field model is the closest to our observation in term of geoid gradient

255   (details of this validation are available in Appendix E). At each pass, we therefore use this model to determine the geoid gradient to be applied.

In the end, the altimetric sea level time series at our comparison point is given by:

$$SSH_{alt} = H - R' - \Delta R_{iono} - \Delta R_{tropo} - \Delta R_{SSB} - \Delta R_{geo} + \Delta R_{geoïd} \tag{3}$$

260

The corrections used to derive the SSH_{alt} are summarised in Table 2.

Table 2. Altimetric corrections used to derive the SSH

Parameter		Correction used
Ionosphere (ΔR_{iono})		GDR Ionospheric mean delay between [-23.85°; -22.5°]
Troposphere (ΔR_{tropo})	Dry	1Hz GDR correction linearly interpolated at the 20 Hz measurements
	Wet	Radiometer / ECMWF model / GNSS Corrections linearly interpolated at the 20 Hz measurements
Sea State Bias (ΔR_{SSB})		1Hz GDR correction linearly interpolated at the 20 Hz measurements
Geophysical (ΔR_{geo})	Ocean tide loading	
	Earth tide	
	Pole tide	
Geoïd gradient ($\Delta R_{geoïd}$)		XGM 2019e gravity field model (Zingerle et al., 2020)

4.2 Altimetric bias computation

The determination of the altimeter bias ($\Delta Bias_{alt}$) consists of comparing the satellite observations (SSH_{alt} from Eq. (3)) with the *in situ* measurements ($SSH_{in\ situ}$ from Eq. (1)) at the time of the overfly (Bonnefond et al., 2011) :

$$Bias_{alt} = SSH_{alt} - SSH_{in\ situ} \tag{4}$$

At each pass, we therefore subtracted the $SSH_{in\ situ}$ from 20 Hz SSH_{alt}. All measurements within ± 1 km (about ± 0.08 s) from our comparison point are averaged to obtain a mean bias and an indicator of the altimeter bias dispersion. This allows us to reject cycles where the standard deviation of the mean bias is greater than 10 cm. We also integrate an altimetry data quality indicator using the range Mean Quadratic Error (MQE). In the altimetry process, the retracking step allow to determine the range by fitting a theorical model on the radar echo recorded by the altimeter. The MQE give an idea of the retracking result: the closer the MQE is to zero, the better the chosen model reproduce the measured waveform. After analysing MQE values on along-track data (more details in Appendix F), we decide to remove cycles where the MQE average exceeds the threshold value of 0.01.

4.2.1 Impact of the wet tropospheric correction

To determine the most appropriate solution for the wet tropospheric correction, we compute the altimetric bias for the Jason 3 track #162 and the 2 Sentinel-3a tracks over the [2016-2021] period, by varying only the wet tropospheric parameter. Figure 6 thus represents the altimetric bias at the comparison point by using the wet tropospheric correction from the radiometer (black), the ECMWF model (grey) and the GNSS based solution (purple). Finally, none of these three corrections significantly improves the dispersion of the results. The radiometer corrections agree with the GNSS-based corrections at the centimetric level, although the GNSS-based corrections slightly decrease the value of the mean altimeter bias. These results confirm that the latest improvements in radiometer corrections now included in the GDR files can be used to derive a consistent altimeter bias. A similar conclusion was made by Bonnefond et al. (2019) at the Corsica historical Cal/Val site for Jason missions. Since GNSS data are not available for all cycles, we chose to keep the wet tropospheric radiometer correction in the following analyses.

4.2.2 Evaluation of the *in situ* SSH determination method

To evaluate our methodology for the $SSH_{in\ situ}$ reconstruction, we compared the mean bias estimated using the 2019x pressure sensor measurements with the one computed using our method (i.e. Eq. 1) over their common observation period (from October 2019 to November 2020). Figure 7 shows the evolution of the altimeter bias for the Jason and Sentinel tracks according to the *in situ* data considered. For the 3 tracks, the difference between the mean biases is a few millimetres (respectively +3/+5/+5 mm for the tracks #162/#359/#458). Despite these small differences, we can notice centimetric variations in the time series of differences (lower right panels, blue curve). This variability can be partly explained by differences in the lagoon hydrodynamic

between the location of the tide gauge and the pressure sensor. Although it is important to take this effect into account for long-term comparisons, we can still assume that the use of the tide gauge series does not affect the estimate of the mean altimeter bias. Our tide gauge data transfer method seems to be relevant for estimating the altimeter bias at the mm-level.

300

Figure 6. Altimetric bias at the comparison point according to different wet tropospheric models and for 3 altimetric tracks: the Jason 3 (orange) track #162, the Sentinel-3a tracks #458 (dark blue) and #359 (light blue) / (a) Altimetric biases distribution as a function of the wet tropospheric delay from the radiometer (black), the ECMWF model (grey) and the GNSS stations (purple). / (b) Bias time differences from the radiometer solution with respect to the ECMWF model (grey) and GNSS stations (purple).
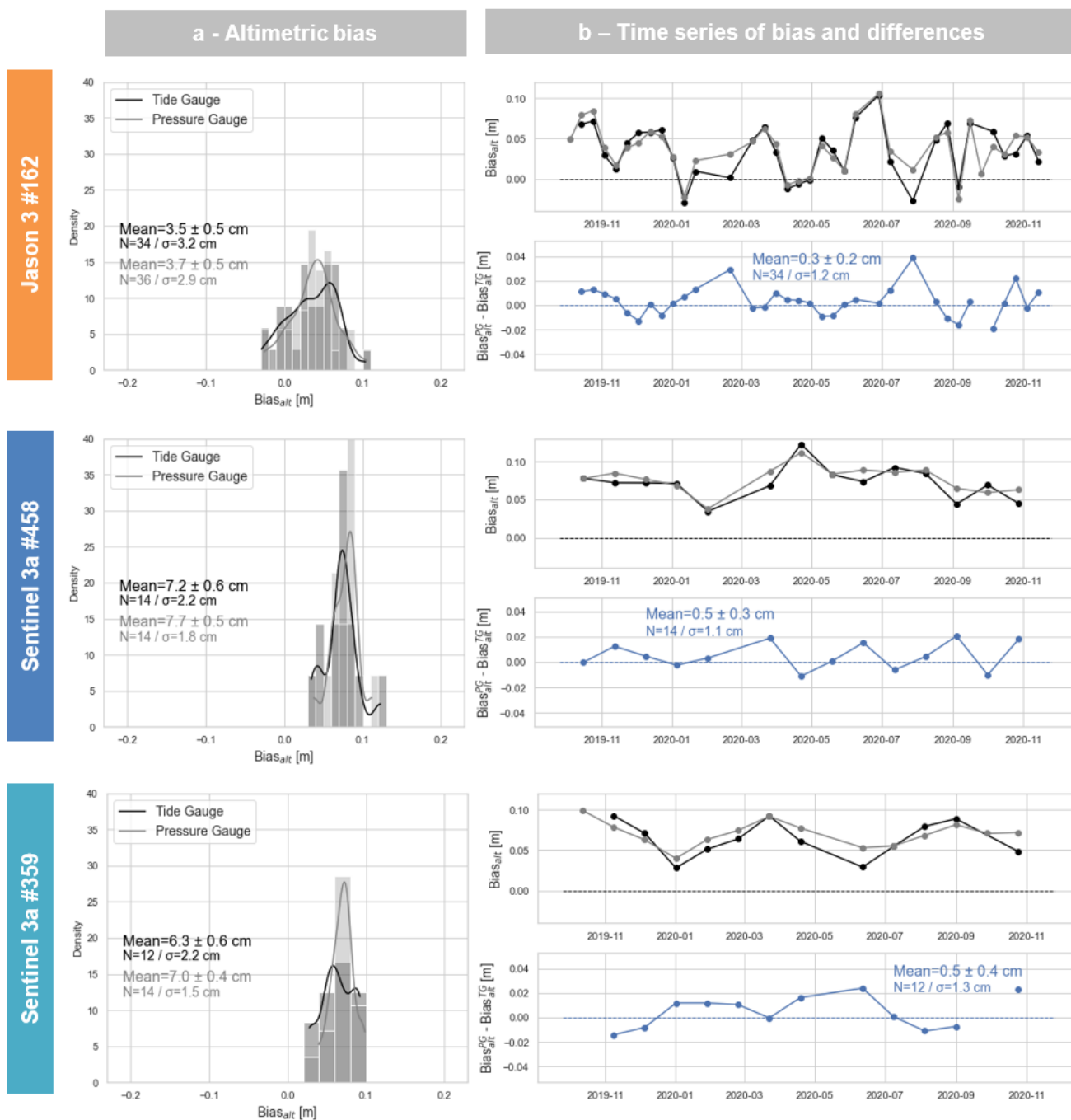
Figure 7. Altimetric bias at the comparison point according to different *in situ* datasets and for 3 altimetric tracks: the Jason 3 (orange) track #162, the Sentinel-3a tracks #458 (dark blue) and #359 (light blue). / (a) Altimetric biases distribution using tide gauge data (black) or 2019x pressure gauge (grey) as *in situ* reference. / (b) Bias time series using tide gauge (black) or pressure gauge (grey) as *in situ* dataset (upper panel) and bias time differences from the pressure sensor (lower panel).

4.2.3 Multi-mission comparison

Since February 2016, the two missions Jason 3 and Sentinel-3a are both measuring sea level over the New Caledonia lagoon

305   with an intersection point close to Noumea, which allows a direct inter-mission comparison. Figure 8 shows the mean altimetric

biases for Jason 3 (+39.3 ± 3.4 mm, orange line) and Sentinel-3a track #359 (+62.4 ± 3.8 mm, light blue line) and #458 (+65.8

± 3.5 mm, dark blue line) at our comparison point between 2016 and 2021. Table 3 summarises the last results of the three

historical Cal/Val sites from the last OSTST session in October 2020 (i.e. Bonnefond et al., 2020; Haines et al., 2020b; Watson

et al., 2020). Comparing to these sites, our altimetric biases are larger by about 48 mm for both Jason 3 and Sentinel-3a. We

310   find an inter-mission bias $[Bias_{alt}^{S3a} - Bias_{alt}^{J3}]$ of +24.8 mm, which is comparable to the inter-mission biases determined at

the Corsica (+24 mm) and Bass-Strait (+30 mm) sites (see Table 3).

Consistency of these results suggests that, rather than data processing problems, there may remain errors in the absolute

referencing and thus in the determination of the $SSH_{in\ situ}$. In this study, the 2019x pressure sensors referencing is mainly

315   based on the GNSS buoy measurements and many factors can influence these results at the centimetric level. These include

the choice of the GNSS processing parameters, inaccuracies related to reference system changes, and the effect of the tether

tension on the buoyancy as recently demonstrated at Bass Strait site (Zhou et al., 2020). Regarding the pressure sensor

measurements, the use of erroneous atmospheric pressures or a mis-modelled trend could also have a significant impact.

Finally, although we show that our tide gauge data transfer method is relevant (see Section 4.2.2), there may still remain some

320   unaccounted-for dynamic processes between the tide gauge and the comparison point that may lead to inaccuracies. To

consolidate the vertical datum, new geodesy measurements sessions could be conducted to reduce uncertainties in the

$SSH_{in\ situ}$ estimation and better constrain the altimeter biases.

4.2.4 Long-term altimetric bias evolution

Using the Noumea tide gauge data, we computed the Jason altimeter bias for all data from 2002 to 2021. The absolute bias

325   estimates from our study are detailed in Fig. 9 for Jason 1 (+90.2 ± 2.6 mm), Jason 2 (+65.2 ± 3.0 mm) and Jason 3 (+39.3 ±

3.4 mm). As for Sentinel-3a, these values are higher than those observed at historical calibration sites (Table 3). When

comparing to the Corsica and Bass Strait sites which are in really good agreement (see Table 3), our results show a mean

difference of about +46mm (J1), +48mm (J2) and +46mm (J3). When regarding the resulting inter-mission biases, we find -

25 mm for J2/J1 and -25.9 mm for J3/J2, which is close to the resulting inter-mission bias for Corsica (resp. -27 and -23 mm)

330   and Bass-Strait sites (resp. -27 and -26 mm). These results are very encouraging and show the interest of the Noumea site to

conduct further Cal/Val activities. As discussed previously, a more robust referencing of the *in situ* data could lead to the

determination of better constrained biases.
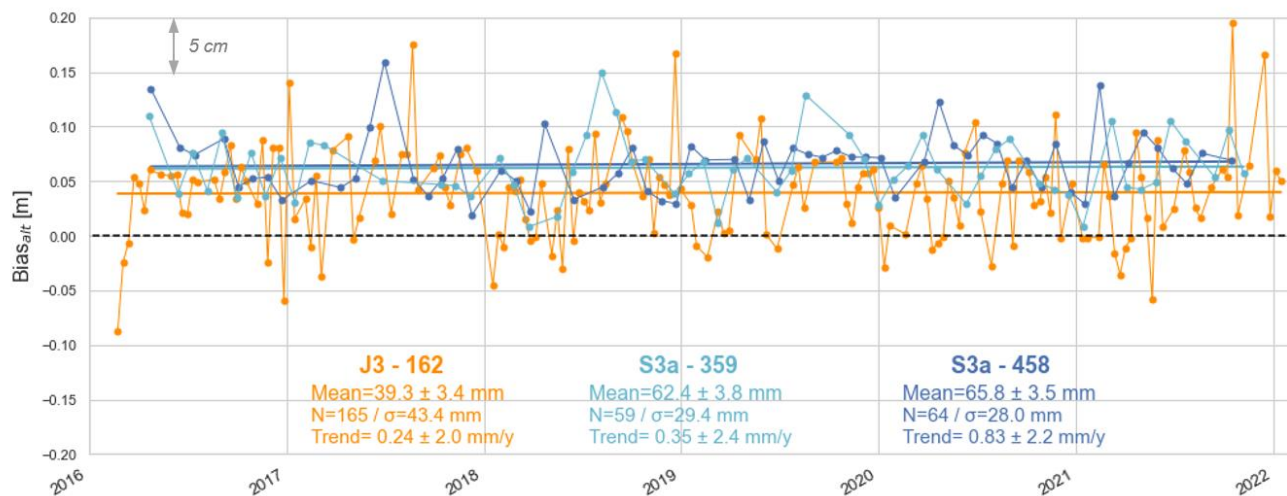
Figure 8. Altimeter bias time series at the comparison point for Jason 3 track #162 (orange) and Sentinel-3a tracks #458 (dark blue) and #359 (light blue) during their common flying period.

335 To the first order, the altimeter bias, differences between altimetry sea level variations and those seen by tide gauge (see Eq. 4), can be related to Vertical Land Motion (VLM) at the tide gauge site (Wöppelmann and Marcos, 2016). We therefore analysed the linear trend estimated on our altimeter bias time series to compare with the vertical motions of nearby GNSS stations. In order to create the longest possible time series, we applied our inter-mission bias (i.e. -25 mm for J2/J1 and -25.9 mm for J3/J2) to realign the datasets to Jason 3 measurements. Over the whole Jason period (2002-2021), a linear trend of -

340 0.13± 0.12 mm/year is estimated. To get a more robust estimate of this trend, we used a bootstrapping method, which consists in estimating the trend 200 times on a random sample of 85% of the original series. It is important to note that this trend is sensitive to the inter-mission biases applied: for example, using Bass Strait inter-mission biases (i.e. -27/-26 mm instead of - 25/-25.9 mm), a zero linear trend is estimated.

345 This being said, our results do not show any significant uplift in Noumea. This differs from the conclusions of Aucan et al. (2017), that find an uplift of +1.41 ±0.67 mm/y over the altimetric period [1993-2013] inferred from the difference between satellite altimetry and tide gauge. The difference likely originates in the method used by Aucan et al. (2017), where the satellite altimetry time series was extracted from a multi-mission gridded dataset at a point far outside the lagoon, before being compared to the tide gauge. Section 4.2.2 showed that, even being only a few km apart, there is SSH differences between the

350 tide gauge and the pressure sensor: the difference with a point outside the lagoon can therefore be even greater. By using along track altimetry products and a closer comparison point, our approach led to a (slightly) different conclusion than the one of the previous study of Aucan et al. (2017), which might be erroneous.

Regarding the VLM, Ballu et al. (2019) found an average subsidence of -1.5 ±0.3 mm/y in the area from nearby permanent
355 GNSS stations, which slightly differs from our conclusions. However, authors also show that this VLM estimation can be very
sensitive to the integration (or not) of a discontinuity in the time series. To solve the question of long-term sea level change in
the lagoon, further studies are thus needed on GNSS data analysis as well as on altimetry and tide gauges. For example,
extending our time series with TOPEX/Poseidon or Sentinel-6 observations would give us a longer and more robust trend
estimate. Having longer observations from the GNSS permanent station collocated with Noumbo tide gauge could also help
360 to constrained vertical land movements at tide gauge.
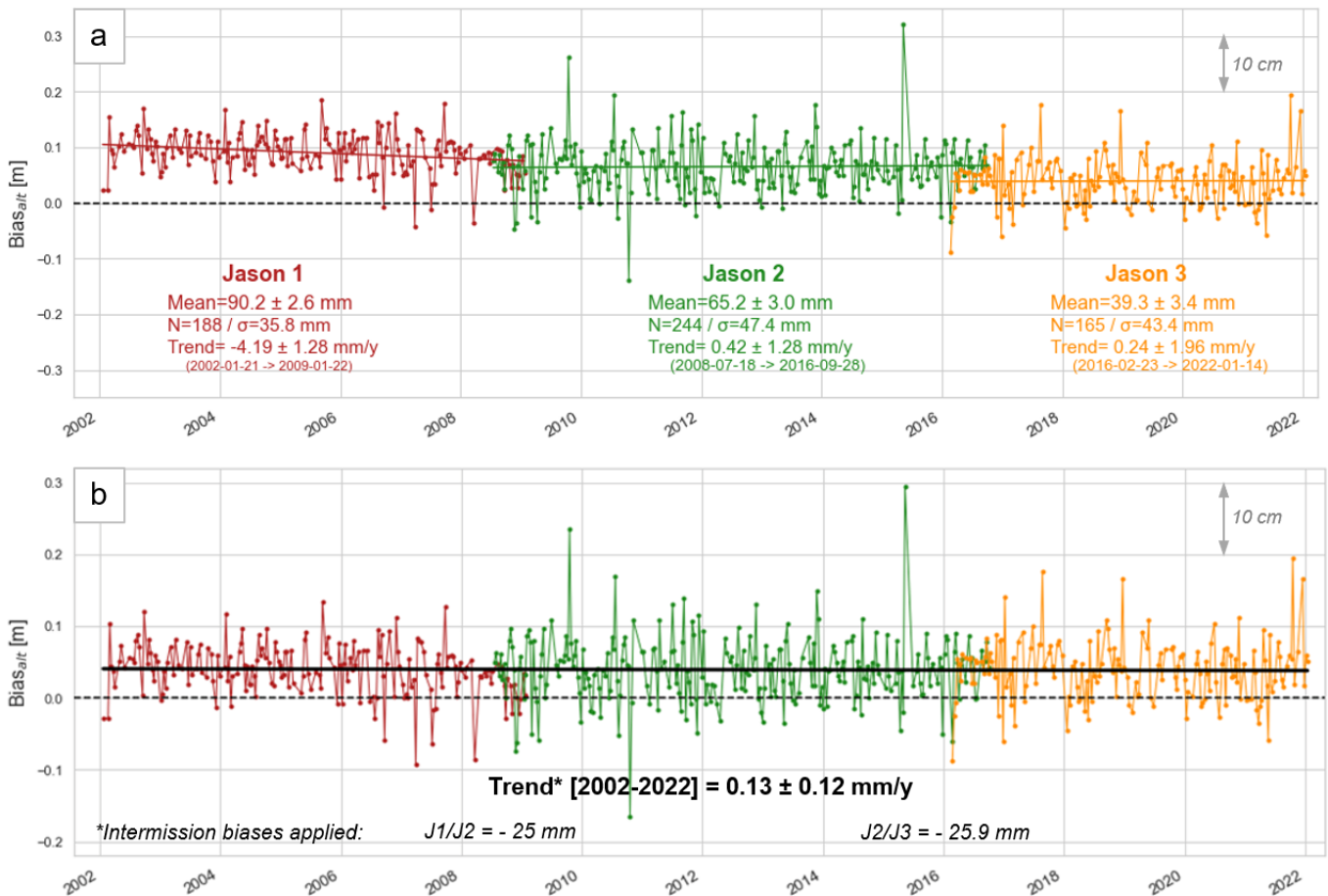
Figure 9. (a) Altimeter bias time series at the comparison point for Jason 1 (red), Jason 2 (green) and Jason 3 (orange) track #162. / (b) Altimeter bias time series after applying inter-missions biases found in this study (i.e. -25 mm for J2/J1 and -25.9 mm for J3/J2) and associated trend over period [2022-2022].

5. Conclusion

In this paper, we demonstrate the potential of the New Caledonia lagoon near Noumea to host Cal/Val activities. Using *in situ*
365 data acquired as part of the GEOCEAN-NC campaign, this study proposes a method to link and compare observations from
the Noumea long-term tide gauge site with an offshore altimetry crossover point from Jason and Sentinel-3a missions. With
measurements from a GNSS buoy and a bottom pressure sensor, we were able to virtually transfer long-term Noumea tide
gauge data to this intersection. A comparison over the common year of measurement of the tide gauge and the pressure sensor
show that this method is relevant for estimating an altimeter bias at the mm-level. The use of along-track altimetry product
370 allows us to test and adapt altimeter correction parameters, especially for the wet tropospheric delay. We consider the up-to-
date GDR parameters and thanks to an SSH survey with CalNaGeo, we validated the use of the XGM2019 gravity field model
to account for geoid gradients.

All these improvements made it possible to compute an accurate altimeter bias time series. For both Jason 1/2/3 and Sentinel-
375 3a missions, we found mean absolute bias higher than historical Cal/Val sites, but the inter-mission biases are very consistent
with those from Bass-Strait and Corsica sites (see Table 3). These results are very encouraging, and additional geodetic
measurements at the crossover could consolidate the vertical datum and better constrain the absolute bias estimate. In the
future, this site also gives the opportunity to reanalyse data from the TOPEX/Poseidon to the recent Sentinel-6 missions.
Extending the comparison will allow to answer new questions, and particularly try to reconcile the sea level trends seen by
380 altimetry, tide gauges and terrestrial permanent GNSS stations. It is also possible to transpose our method to other study areas,
thus increasing the potential number of Cal/Val sites around the world. However, as in Noumea, these new areas must have
suitable altimetry data in the vicinity of a long-term tide gauge site, as well as a hydrodynamic context conducive to the
realization of a geodetic mission (navigation, sensors deployment…).

385 Finally, although the GEOCEAN-NC campaign is not directly related to the preparation of the future SWOT mission, a better
knowledge of the lagoon dynamic and the mapping of the fine-scale geoid will be useful for the exploitation of its future large-
swath measurements. Thus, the Noumea lagoon represents a real opportunity to establish an absolute and relatively low-coast
Cal/Val site, to better understand current and future altimetry data.

390

Table 3. Altimetric mean biases and inter-mission biases for Jason 1-2-6 and Sentinel-3a missions for three historical Cal/Val sites and the Noumea lagoon (Harvest, Corsica and Bass Strait results are extract from the last OSTST sessions, 20-22 October 2020)

		Jason 1	**Jason 2**	**Jason 3**	**Sentinel-3a**
Harvest (Haines et al., 2020b)	*Products*	GDR-E	GDR-D	GDR-D	-
	Cycles	-	-	-	-
	Bias	+6 ± 2 mm	+5 ± 3 mm	-12 ± 3 mm	-

		Jason 1	**Jason 2**	**Jason 3**	**Sentinel-3a**
Corsica (Bonnefond et al., 2020)	*Products*	GDR-E	GDR-D	GDR-T	NTC, BC4
	Cycles	1-259	1-305	1-165	3-60
	Bias	+43 ± 3 mm	+16 ± 2 mm	-7 ± 3 mm	+17 ± 4 mm
Bass Strait (Watson et al., 2020)	*Products*	GDR-E	GDR-D	GDR-D	NTC, BC4
	Cycles	1-259	1-298	1-166	3-62
	Bias	+45.6 ± 2.2 mm	+18.8 ± 2.1 mm	-6.7 ± 2.3 mm	+24.4 ± 2.0 mm
Inter-mission bias		-	-27 mm	-24 mm	+31 mm	-

		Jason 1	**Jason 2**	**Jason 3**	**Sentinel-3a**
Noumea	*Products*	GDR-E	GDR-D	GDR-F	NTC, BC4
	Cycles	1-259	1-303	1-219	3-81
	Bias	+90.2 ± 2.6 mm	+65.2 ± 3.0 mm	+39.3 ± 3.4 mm	+62.4 ± 3.8 mm (#359) +65.8 ± 3.5 mm (#458)
Inter-mission bias		-	-25.0 mm	-25.9 mm	+24.8 mm	-

Author contribution

395 C.C., V.B., L.T. and Y.-T.T. designed the study, V.B, C.C. and J.A. designed and conducted the field campaign, C.C. processed the data and wrote the original draft of the paper. Writing—review & editing, C.C., V.B., L.T., Y.-T.T. and J.A. All authors have read and agreed to the published version of the manuscript.

Data availability

Navigation data for the 2019 GEOCEAN-NC campaign are available online (https://doi.org/10.17600/18000899). Altimetry
400 products are available for download online (see Section 4.1.1) and sensor data used in this paper are available from the authors upon request.

Competing interests

The authors declare no conflict of interest. The funders had no role in the design of the study; in the collection, analyses, or interpretation of data; in the writing of the manuscript, or in the decision to publish the results.

405 **Funding**

This study has been conducted and funded thanks to Centre National d'Etudes Spatiales (CNES) through the FOAM project of the TOSCA program, Centre National de la Recherche Scientifique (CNRS), and French Ministry of Research. Funding for C.Chupin PhD is provided by the Direction Générale de l'Armement (DGA) and the Nouvelle Aquitaine region.

Acknowledgements

410 For the GEOCEAN-NC mission in Noumea lagoon in October 2019 (DOI : https://doi.org/10.17600/18000899), the authors want to thank Etienne Poirier for the instrument management during the campaign, and the commandant and crew of the R/V Alis. We acknowledge the help of IRD, Shom and DITTT for logistics and on-land tide and GNSS data collection. We also thank the US IMAGO Noumea teams for their logistic support during the campaign, and more particularly Bertrand Bourgeois and Mahé Dumas for the deployment and recovery of the pressure sensors. We acknowledge the CNFC (Comission Nationale
415 de la Flotte Côtière), Ifremer, IRD and the Government of New Caledonia for rapidly adjusting and obtaining permissions for the new cruise plan. We also want to thanks the GINS community and especially the GET laboratory for helping with GNSS computation, and the LEGOS altimetry experts (especially Florence Birol and Fabien Léger) for their help and advices analysing altimetry dataset in the lagoon. The pressure sensor data were analysed using code kindly provided by Marc Pezerat from LIENSs.

References

André, G., Miguez, B. M., Ballu, V., Testut, L., and Wöppelmann, G.: Measuring sea level with gps-equipped buoys: a multi-instruments experiment at Aix Island, Int. Hydrogr. Rev., 26–38, 2013.

Aucan, J., Merrifield, M. A., and Pouvreau, N.: Historical Sea Level in the South Pacific from Rescued Archives, Geodetic Measurements, and Satellite Altimetry, Pure Appl. Geophys., 174, 3813–3823, https://doi.org/10.1007/s00024-017-1648-1, 2017.

Babu, K. N., Shukla, A. K., Suchandra, A. B., Arun Kumar, S. V. V., Bonnefond, P., Testut, L., Mehra, P., and Laurain, O.: Absolute Calibration of SARAL/AltiKa in Kavaratti During its Initial Calibration-Validation Phase, Marine Geodesy, 38, 156–170, https://doi.org/10.1080/01490419.2015.1045639, 2015.

Ballu, V.: GEOCEAN-NC cruise - RV Alis, https://doi.org/10.17600/18000899, 2019.

Ballu, V., Bonnefond, P., Calmant, S., Bouin, M.-N., Pelletier, B., Laurain, O., Crawford, W. C., Baillard, C., and de Viron, O.: Using altimetry and seafloor pressure data to estimate vertical deformation offshore: Vanuatu case study, Advances in Space Research, 51, 1335–1351, https://doi.org/10.1016/j.asr.2012.06.009, 2013.

Ballu, V., Gravelle, M., Woppelmann, G., de Viron, O., Rebischung, P., Becker, M., and Sakic, P.: Vertical land motion in the Southwest and Central Pacific from available GNSS solutions and implications for relative sea levels, Geophysical Journal International, 218, 1537–1551, https://doi.org/10.1093/gji/ggz247, 2019.

Bonnefond, P., Exertier, P., Laurain, O., Ménard, Y., Orsoni, A., Jeansou, E., Haines, B. J., Kubitschek, D. G., and Born, G.: Leveling the Sea Surface Using a GPS-Catamaran, Marine Geodesy, 26, 319–334, https://doi.org/10.1080/714044524, 2003.

Bonnefond, P., Haines, B. J., and Watson, C.: In situ Absolute Calibration and Validation: A Link from Coastal to Open-Ocean Altimetry, in: Coastal Altimetry, edited by: Vignudelli, S., Kostianoy, A. G., Cipollini, P., and Benveniste, J., Springer Berlin Heidelberg, Berlin, Heidelberg, 259–296, https://doi.org/10.1007/978-3-642-12796-0_11, 2011.

Bonnefond, P., Exertier, P., Laurain, O., Thibaut, P., and Mercier, F.: GPS-based sea level measurements to help the characterization of land contamination in coastal areas, Advances in Space Research, 51, 1383–1399, https://doi.org/10.1016/j.asr.2012.07.007, 2013.

Bonnefond, P., Exertier, P., Laurain, O., Guinle, T., and Féménias, P.: Corsica: A 20-Yr multi-mission absolute altimeter calibration site, Advances in Space Research, https://doi.org/10.1016/j.asr.2019.09.049, 2019.

Bonnefond, P., Exertier, P., Laurain, O., Guinle, T., and Féménias, P.: Corsica: A 20-Yr multi-mission absolute altimeter calibration site, OSTST 2020 virtual meeting, 2020.

Bonnefond, P., Laurain, O., Exertier, P., Calzas, M., Guinle, T., Picot, N., and the FOAM Project Team: Validating a New GNSS-Based Sea Level Instrument (CalNaGeo) at Senetosa Cape, Marine Geodesy, 45, 121–150, https://doi.org/10.1080/01490419.2021.2013355, 2022.

Born, G. H., Parke, M. E., Axelrad, P., Gold, K. L., Johnson, J., Key, K. W., Kubitschek, D. G., and Christensen, E. J.: Calibration of the TOPEX altimeter using a GPS buoy, J. Geophys. Res., 99, 24517, https://doi.org/10.1029/94JC00920, 1994.

Chelton, D. B., Ries, J. C., Haines, B. J., Fu, L.-L., and Callahan, P. S.: Satellite altimetry, Satellite Altimetry and Earth Sciences, 69, 1–131, 2001.

455 Chupin, C., Ballu, V., Testut, L., Tranchant, Y.-T., Calzas, M., Poirier, E., Coulombier, T., Laurain, O., Bonnefond, P., and Team FOAM Project: Mapping Sea Surface Height Using New Concepts of Kinematic GNSS Instruments, Remote Sensing, 12, 2656, https://doi.org/10.3390/rs12162656, 2020.

Crétaux, J.-F., Bergé-Nguyen, M., Calmant, S., Romanovski, V. V., Meyssignac, B., Perosanz, F., Tashbaeva, S., Arsen, A., Fund, F., Martignago, N., Bonnefond, P., Laurain, O., Morrow, R., and Maisongrande, P.: Calibration of Envisat radar altimeter
460 over Lake Issykkul, Advances in Space Research, 51, 1523–1541, https://doi.org/10.1016/j.asr.2012.06.039, 2013.

Douillet, P.: Tidal dynamics of the south-west lagoon of New Caledonia: observations and 2D numerical modelling, Oceanologica Acta, 21, 69–79, https://doi.org/10.1016/S0399-1784(98)80050-9, 1998.

Fund, F., Perosanz, F., Testut, L., and Loyer, S.: An Integer Precise Point Positioning technique for sea surface observations using a GPS buoy, Advances in Space Research, 51, 1311–1322, https://doi.org/10.1016/j.asr.2012.09.028, 2013.

465 Gobron, K., de Viron, O., Wöppelmann, G., Poirier, É., Ballu, V., and Van Camp, M.: Assessment of Tide Gauge Biases and Precision by the Combination of Multiple Collocated Time Series, J. Atmos. Oceanic Technol., 36, 1983–1996, https://doi.org/10.1175/JTECH-D-18-0235.1, 2019.

Gommenginger, C., Thibaut, P., Fenoglio-Marc, L., Quartly, G., Deng, X., Gómez-Enri, J., Challenor, P., and Gao, Y.: Retracking Altimeter Waveforms Near the Coasts, in: Coastal Altimetry, edited by: Vignudelli, S., Kostianoy, A. G., Cipollini,
470 P., and Benveniste, J., Springer Berlin Heidelberg, Berlin, Heidelberg, 61–101, https://doi.org/10.1007/978-3-642-12796-0_4, 2011.

Gourdeau, L., Cravatte, S., and Marin, F.: Internal tides and mesoscale interactions in a tropical area: insights from model, in situ data, and SWOT, 2020.

Haines, B., Desai, S. D., Kubitschek, D., and Leben, R. R.: A brief history of the Harvest experiment: 1989–2019, Advances
475 in Space Research, https://doi.org/10.1016/j.asr.2020.08.013, 2020a.

Haines, B., Desai, S., Desjonquères, J.-D., Talpe, M., Leben, B., Gourmos, A., Meinig, C., and Stalin, S.: The Harvest Experiment: New Results and Status on the Eve of Sentinel-6 Launch, OSTST 2020 Virtual meeting, 2020b.

Hersbach, H., Bell, B., Berrisford, P., Biavati, G., Horányi, A., Muñoz Sabater, J., Nicolas, J., Peubey, C., Radu, R., Rozum, I., Schepers, D., Simmons, A., Soci, C., Dee, D., and Thépaut, J.-N.: ERA5 hourly data on pressure levels from 1979 to present,
480 Copernicus Climate Change Service (C3S) Climate Data Store (CDS), 2018.

Imel, D. A.: Evaluation of the TOPEX/POSEIDON dual-frequency ionosphere correction, J. Geophys. Res., 99, 24895, https://doi.org/10.1029/94JC01869, 1994.

Kouba, J.: Implementation and testing of the gridded Vienna Mapping Function 1 (VMF1), J Geod, 82, 193–205, https://doi.org/10.1007/s00190-007-0170-0, 2008.

485 Lemoine, J.-M., Biancale, R., Reinquin, F., Bourgogne, S., and Gégout, P.: CNES/GRGS RL04 Earth gravity field models, from GRACE and SLR data, https://doi.org/10.5880/ICGEM.2019.010, 2019.

Martínez-Asensio, A., Wöppelmann, G., Ballu, V., Becker, M., Testut, L., Magnan, A. K., and Duvat, V. K. E.: Relative sea-level rise and the influence of vertical land motion at Tropical Pacific Islands, Global and Planetary Change, 176, 132–143, https://doi.org/10.1016/j.gloplacha.2019.03.008, 2019.

490   Marty, J. C., Loyer, S., Perosanz, F., Mercier, F., Bracher, G., Legresy, B., Portier, L., Capdeville, H., Fund, F., Lemoine, J. M., and Biancale, R.: GINS: The CNES/GRGS GNSS scientific software, in: ESA Proceedings WPP326, 3 rd International Colloquium Scientific and Fundamental Aspects of the Galileo Programme, Copenhagen, Denmark, 2011.

Mertikas, S., Donlon, C., Féménias, P., Mavrocordatos, C., Galanakis, D., Tripolitsiotis, A., Frantzis, X., Tziavos, I., Vergos, G., and Guinle, T.: Fifteen Years of Cal/Val Service to Reference Altimetry Missions: Calibration of Satellite Altimetry at the
495   Permanent Facilities in Gavdos and Crete, Greece, 10, 1557, https://doi.org/10.3390/rs10101557, 2018.

Nerem, R. S., Haines, B. J., Hendricks, J., Minster, J. F., Mitchum, G. T., and White, W. B.: Improved determination of global mean sea level variations using TOPEX/POSEIDON altimeter data, Geophys. Res. Lett., 24, 1331–1334, https://doi.org/10.1029/97GL01288, 1997.

Pavlis, N. K., Holmes, S. A., Kenyon, S. C., and Factor, J. K.: The development and evaluation of the Earth Gravitational
500   Model 2008 (EGM2008), J. Geophys. Res., 117, https://doi.org/10.1029/2011JB008916, 2012.

Saastamoinen, J.: Atmospheric Correction for the Troposphere and Stratosphere in Radio Ranging Satellites, in: Geophysical Monograph Series, edited by: Henriksen, S. W., Mancini, A., and Chovitz, B. H., American Geophysical Union, Washington, D. C., 247–251, https://doi.org/10.1029/GM015p0247, 1972.

Vondrak, J.: Problem of Smoothing Observational Data II, 28, 84–89, 1977.

505   Watson, C., White, N., Church, J., Burgette, R., Tregoning, P., and Coleman, R.: Absolute Calibration in Bass Strait, Australia: TOPEX, Jason-1 and OSTM/Jason-2, Marine Geodesy, 34, 242–260, https://doi.org/10.1080/01490419.2011.584834, 2011.

Watson, C., Legresy, B., Beardsley, J., and King, M.: Altimeter validation results from the Bass Strait validation facility, Australia, OSTST 2020 Virtual meeting, 2020.

Willis, J.: Report of the 2011 Ocean Surface Topography Science Team Meeting., 2011.

510   Wöppelmann, G. and Marcos, M.: Vertical land motion as a key to understanding sea level change and variability, Rev. Geophys., 54, 64–92, https://doi.org/10.1002/2015RG000502, 2016.

Zhou, B., Watson, C., Legresy, B., King, M. A., Beardsley, J., and Deane, A.: GNSS/INS-equipped buoys for altimetry validation: lessons learnt and new directions from the Bass Strait validation facility, 12, 3001, https://doi.org/10.3390/rs12183001, 2020.

515   Zingerle, P., Pail, R., Gruber, T., and Oikonomidou, X.: The combined global gravity field model XGM2019e, J Geod, 94, 66, https://doi.org/10.1007/s00190-020-01398-0, 2020.

Zumberge, J. F., Heflin, M. B., Jefferson, D. C., Watkins, M. M., and Webb, F. H.: Precise point positioning for the efficient and robust analysis of GPS data from large networks, J. Geophys. Res., 102, 5005–5017, https://doi.org/10.1029/96JB03860, 1997.

520

Appendices

Appendix A - GEOCEAN-NC pressure gauges calibration

Pressure sensors are known to drift over time. This drift is generally considered to be linear and variable from instrument to
525 instrument, depending on the age and past history of the sensor. In our case, a calibration session in hyperbaric chamber before
and after their deployment do not show a clear instrumental drift of the different sensors (Figure A1c).

To verify the stability of the measurements during the 13 months of immersion, we compute relative differences with the
2019o sensor (Figure A1d). This sensor was chosen as a reference because of its installation on a stable support (coral reef),
530 and we consider its instrumental drift negligible regarding the previous calibration session. Results show that, for sensors 2019i
and 2019j (Figure A1d, in green and yellow), differences do not show a significant trend: therefore, it is assumed that these
two sensors remained stationary.

On the contrary, the 2019o/2019r difference (Figure A1d, in red) shows a negative trend for the first 7 months, before
535 stabilizing in May 2020. This suggests a sinking of the sensor into the sand, which was confirmed by the divers during the
gauge's recovery. The nature of the bottom is therefore a parameter to consider when deploying the sensors. If the experimental
conditions impose an installation on very soft grounds, other types of support can also be considered (suction anchors, etc.).
Finally, the 2019o/2019x difference (Figure A1d, blue) shows a linear trend of about -70 mm/yr, which is not visible on the
other sensors nor conceivable from the pre- and post-deployment drift checks. This could indicate continued sensor sinking,
540 and in the absence of further information, we chose to correct for this trend in the following study.

(a)

(b)

(c)

(d)
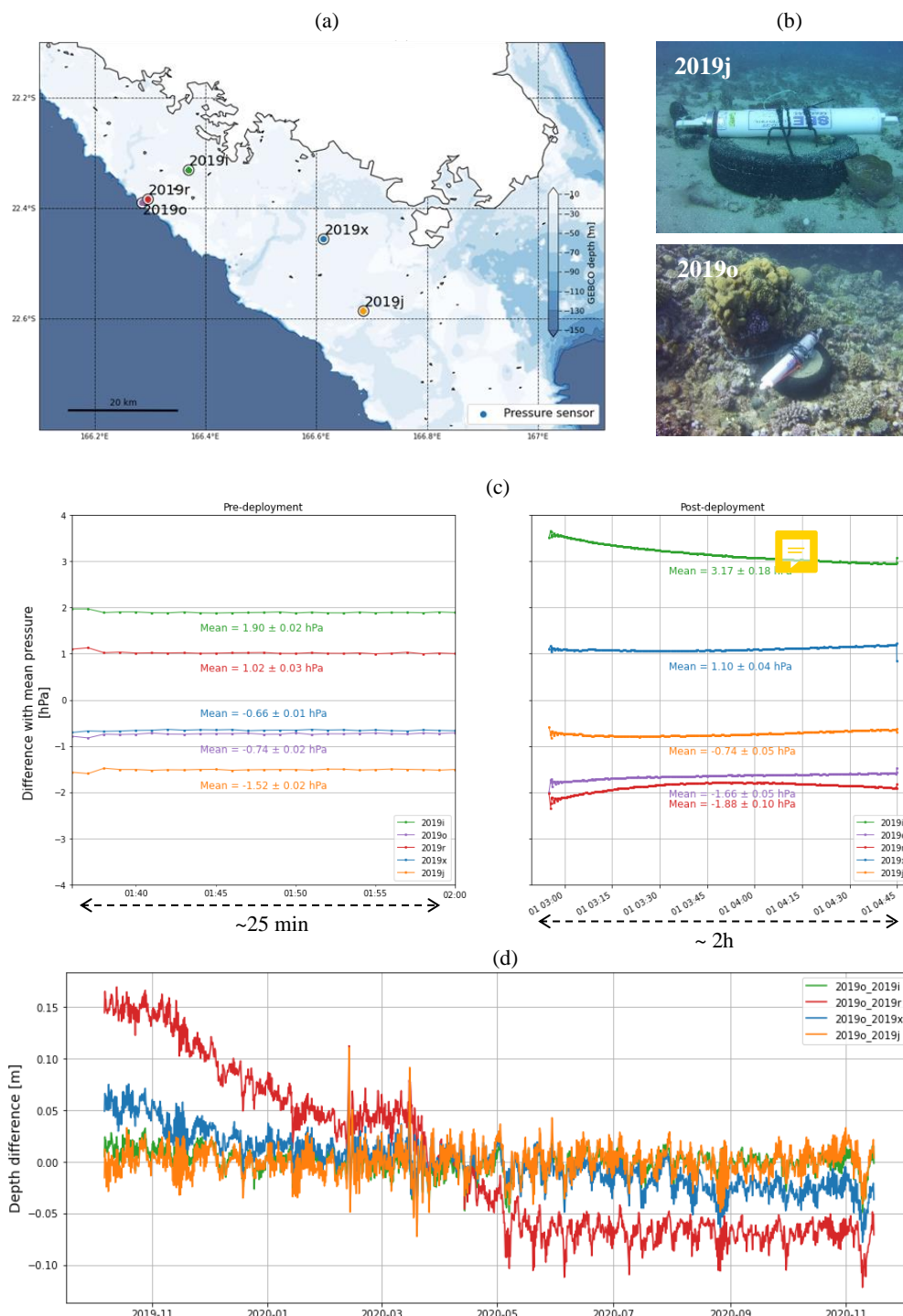
Figure A 1. Installation and calibration phase of the pressure gauges / (a) – (b) Location and mooring of the 5 pressure gauges deployed during GEOCEAN-NC campaign. / (c) Hyperbaric chamber calibration results: difference between SBE observations and mean pressure at 10m before (left) and after (right) deployment. For conversion, 1 hPa ~ 1 cm of water. / (d) Difference between the 2019o sensor time series and the other 4 pressure sensors. The pressure time series were transformed into equivalent water depths and then corrected for tide using harmonic analysis. The final differences were filtered with a sliding average (6 h windows, 6 h steps).

Appendix B - GNSS processing parameters

545

Table B 1. GINS parameters for GNSS computation

	GNSS Buoy	CalNaGeo GNSS carpet
Constellation	GPS / GLONASS / GALILEO	GPS / GLONASS / GALILEO
Resolution mode	IPPP / PPP / IPPP	PPP
Observation sampling	10s	10s
Earth parameters	Nominal NRO	Nominal NRO
Ocean tide loading	FES2014	FES2014
Atmosphere loading	Uncorrected	Uncorrected
IONEX file	Default ionosphere	Default ionosphere
Orbit/Clock	MG3	MG3
Macromodel	Nominal MG3	Nominal MG3
ANTEX	igsR3.atx	igsR3.atx
Elevation mask	15	15
Minimum visible satellite	4	4
Minimum satellite pass duration	300 s	350 s
Epochs deleted at each pass start	2 (20 sec)	2 (20 sec)
Minimum pass length for integer ambiguity computation	600 s	-
Kalman filter	Yes	Yes

Appendix C - Sea State Comparison between GNSS Buoy and 2019x pressure sensor

To be sure that our GNSS buoy and the 2019x pressure sensor monitor the same sea, we compare the Significant Wave Heights (SWH) from both instruments.

SWH from the GNSS buoy

Located at the water surface, the GNSS buoy observations are directly impacted by the sea state, but also by longer variations such as tide or the geoid. To process theses data, we used the method describe in Bonnefond et al. (2003). To focus on the short variations, we differentiate between the filtered and the raw buoy data (RTKLib 1Hz differential solution). For that, GNSS heights are processed using the Vondrak filter (Vondrak, 1977) with a cut-off period of 120s to remove short-wavelength oscillations (Figure C1-a). Standard deviation of these residuals' heights (σ_{shr}) is compute using a 120s period's running average (Figure C1-b). The standard deviation of the buoy due to waves (σ_{wave}) is then equal to : $\sigma_{wave} = \sqrt{\sigma_{shr}^2 + \sigma_{gps}^2}$ with σ_{gps} the internal errors of the GNSS buoy measurements (here estimate to be 2.5cm). The final Significant Wave Height (SWH) at the buoy is then derived from: $SWH = 4 \times \sigma_{wave}$ (Figure C1-c).

SWH from the 2019x pressure sensors

The SBE26plus sensors have been set up to measure wave bursts during 10 minutes every hour (with 1 second wave sample duration). To compute the resulting SWH from theses wave bursts at 2019x, we first transform pressure records to equivalent hydrostatic depths using atmospheric pressure from Magenta Airport, temperature from pressure recorder and a mean salinity of 35.5 psu. Then, we remove a linear trend for each burst of 512 values and reconstruct waves elevation. The Power Spectrum Density (PSD) is then estimated and the final waves parameters are extracted. After several tests, we choose a cut-off frequency of Fc=0.25 Hz. In order to easily compare with GNSS buoy SWH, this method is applied to the buoy observations, after selecting the same observation windows as from the pressure sensor's wave bursts.

Comparison

The results of the GNSS Buoy and 2019x pressure sensor SWH computation are showed in Figure We can see that the GNSS buoy, measuring at the direct water surface, is very sensitive to waves, down to frequency bands of 0.5Hz. If we apply the same cut-off frequency as the bottom pressure sensor (Fc=0.25) to the buoy data, we obtain a high correlation between the two series (c= 0.919, Figure C4). Thus, at a depth of around 20 m, the pressure sensor is limited to a narrower frequency band than the buoy. But if we limit the comparison at the frequency band common to both systems, they roughly see the same sea.
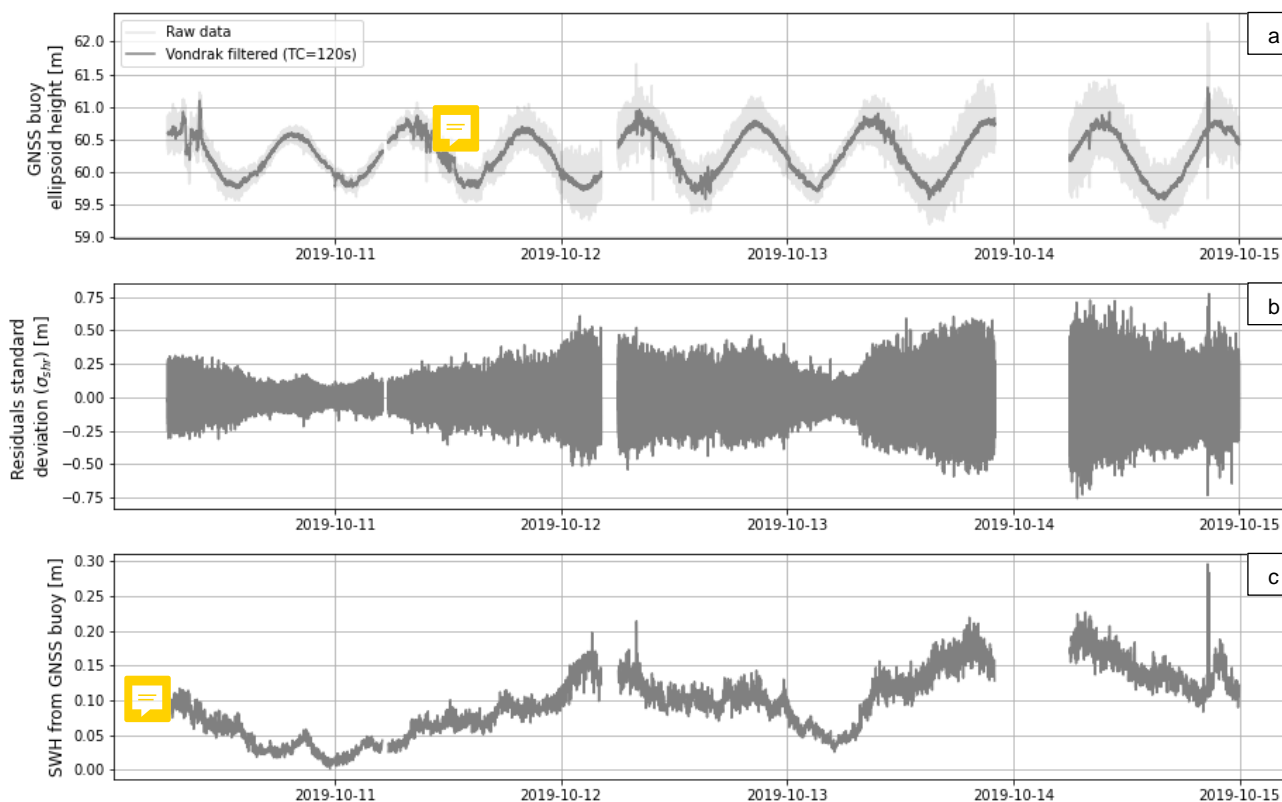
Figure C 1. Computation step of the GNSS Buoy SWH / (a) Raw and Vondrak filtered GNSS buoy ellipsoid heights / (b) Standard deviation of these residuals' heights (σ_{shr}) / (c) Significant Wave Height (SWH) at the buoy position.

580
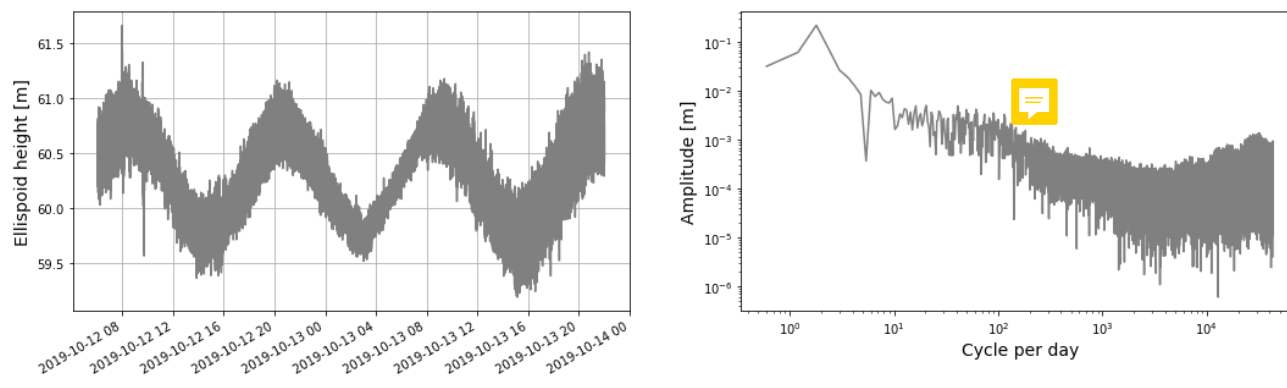
Figure C 2. FFT computation for GNSS buoy observations of the 12th - 13th October 2019.
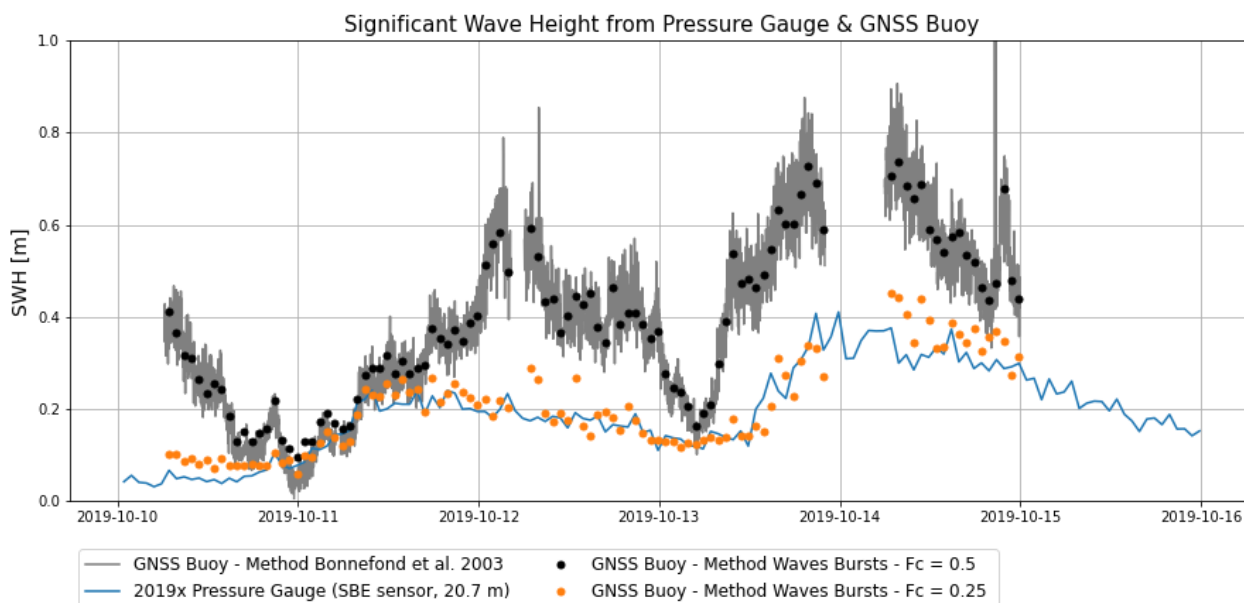
Figure C 3. Significant Wave Height from GNSS Buoy (grey line) and 2019x pressure gauge (blue line). To allow direct comparison, the
585   GNSS Buoy SWH is also compute with the wave burst method, using different cut-off frequencies (black and orange points).
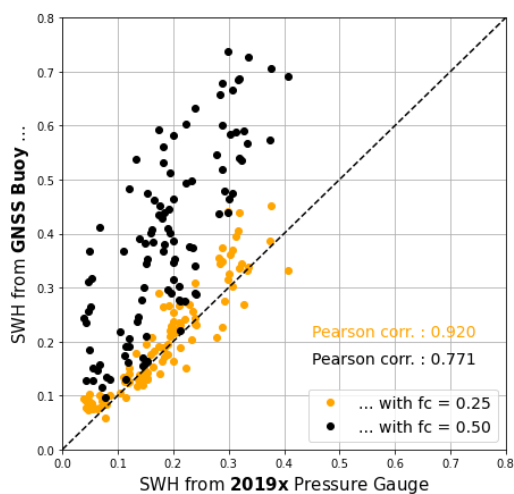
Figure C 4. Correlation between 2019x Pressure Gauge and GNSS Buoy SWH.

590 **Appendix D – Along-track altimetric wet tropospheric corrections**

In the lagoon, the effect of coastal contamination on the radiometer data is visible when approaching the main island (Figure D1, grey area). However, the wet tropospheric correction seems to be exploitable at our comparison point for all missions (Figure D1, red area).

595
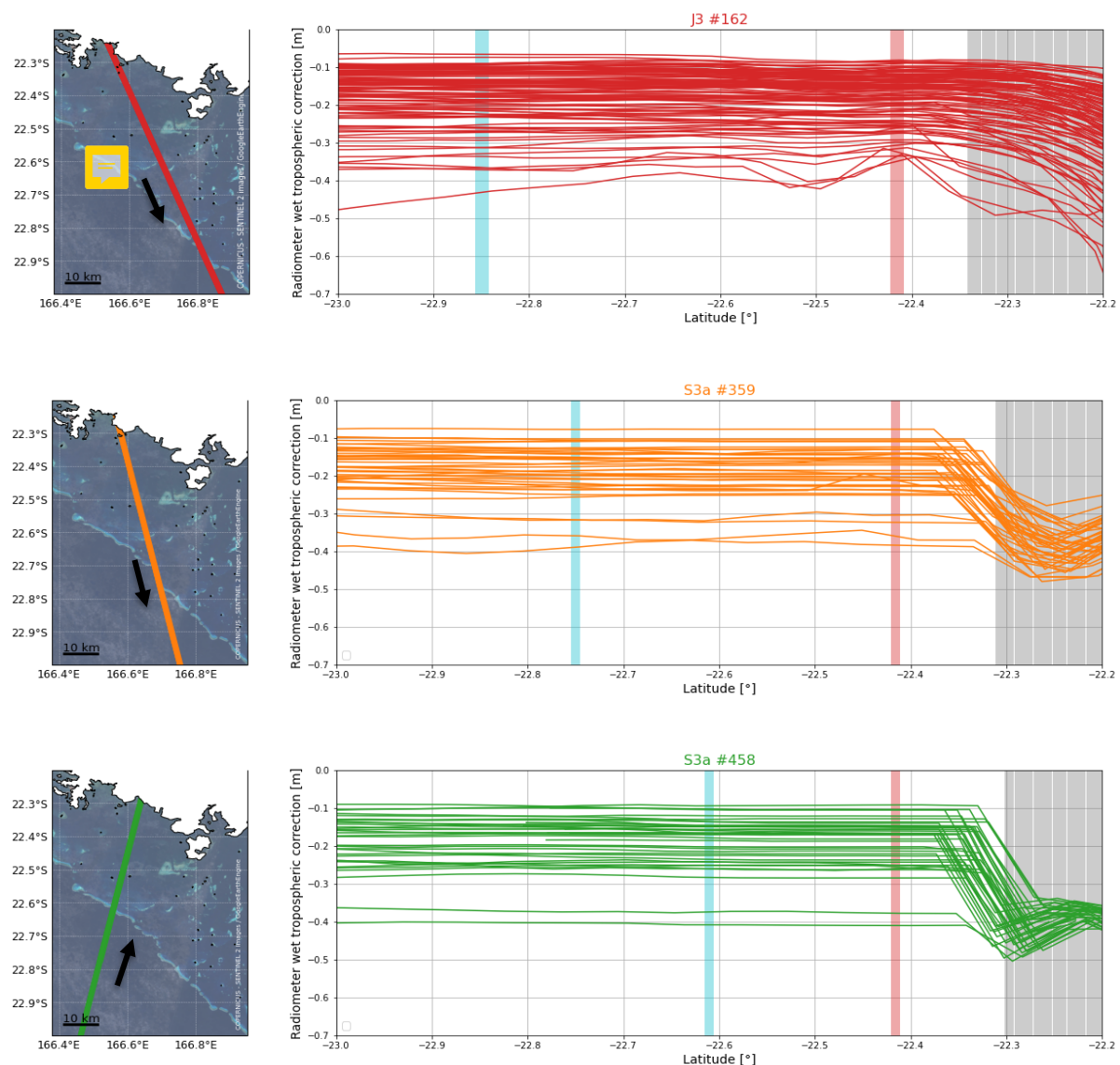
Figure D 1. Evolution of the radiometer correction along the three altimetric tracks used in our study (red for Jason 3 #162, orange for Sentinel-3a #359 and green for Sentinel-3a #458). The grey vertical bar represents the main island overfly, the red vertical bar represents the comparison point location and the blue vertical bar corresponds to the reef barrier overfly.

To test this hypothesis, we compared the correction provided by the radiometer with two data sets: (1) the wet tropospheric correction from the ECMWF model and (2) the wet tropospheric correction computed from permanent GNSS stations in Noumea. For the latter, we used the total tropospheric delay extracted from GINS PPP computations, performed by the CNES

600   teams in Toulouse, for the NRMD and NOUM stations. The tropospheric corrections, estimated every 2 hours, are interpolated at the satellite pass times. The dry tropospheric component from GDR files is then subtracted to finally obtain the wet component of the tropospheric correction. Since the GNSS stations are not at sea level elevation, an additional correction is applied to account for the pressure difference with the comparison point (which is at sea level elevation). For this, we used the Saastamoinen equations (Saastamoinen, 1972) according to the method described by Kouba (2008).

605

To illustrate the objective of our comparison, we represent the wet tropospheric delay from radiometer, ECMWF model and GNSS data along the Jason 3 track #162 for 3 random cycles (Figure D2). If we focus on our study area (the grey area on Figure D2), we can see that the three solutions can be very variable according to the cycles and can affect the estimate of the altimetric SSH at the centimetric level.

610
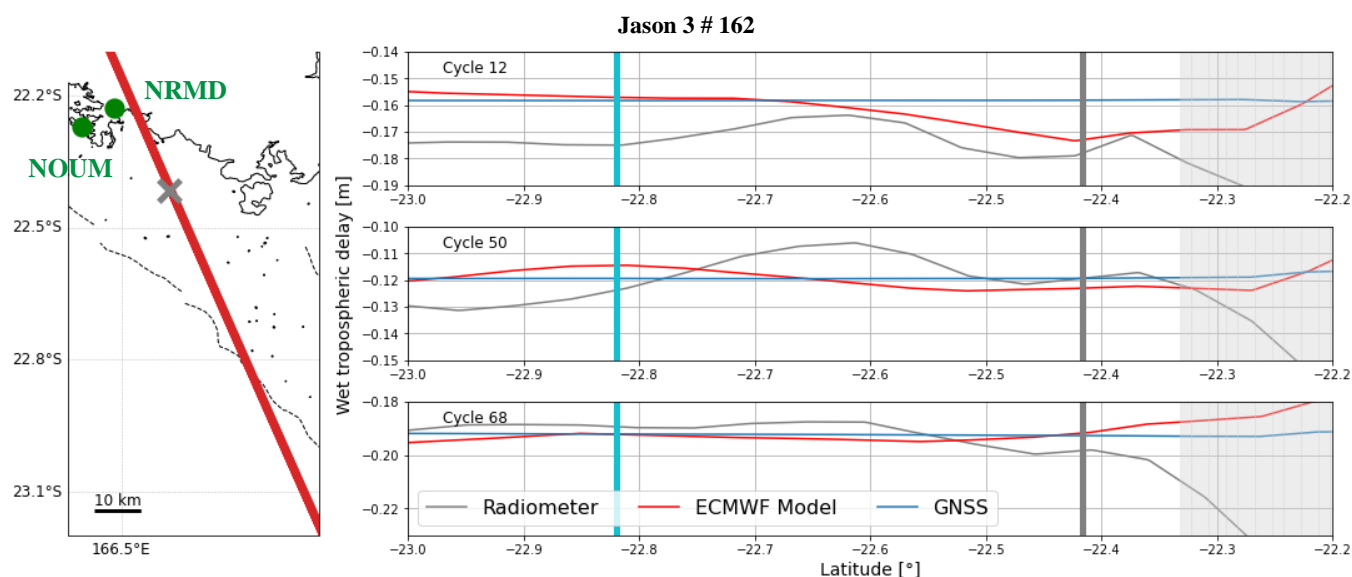
Figure D 2. Wet tropospheric correction from radiometer (grey), ECMWF model (red) and GNSS stations (blue) for three random cycles of the Jason 3 #162. On the right panel, the light grey area represents the main island overfly, the dark grey area represents the comparison point overfly and the blue area corresponds to the reef barrier overfly.

Appendix E - Validation of gradients from global geoïd models in the lagoon

Another objective of the cruise was to improve sea level kinematic mapping methodology in coastal areas through the deployment and comparison of multiple sensors, as described in Chupin et al. 2020. For that purpose, the coastal version of the CalNaGeo GNSS carpet was towed by R/V ALIS along and across altimetry tracks, and inside and outside the lagoon

615 (Figure 1b, blue lines). The 10 s observations of CalNaGeo were processed with GINS in PPP mode (Marty et al., 2011) (processing details in Appendix B), and filtered using the Vondrak filter with a cutoff period of 30 min (~ 5.4 km at 6 knots). The 2019x pressure sensor is then used to remove the time-varying component of CalNaGeo measurements (especially the oceanic tide). Thanks to these data, we then analyse the performance of different models to estimate geoid gradients in our study area.

620 Three datasets were selected to conduct our comparison:

- The XGM2019e global gravity field model (Zingerle et al., 2020), represented by spherical harmonics corresponding to a spatial resolution of 2' (~4 km). This model is based on GOCO06s satellite data combined with terrestrial measurements for shorter wavelengths. Gravity anomalies derived from satellite altimetry are used over oceans (DTU13).

625 - The global Earth gravity potential model EGM2008 (Pavlis et al., 2012) defined on a 5' arc (~10 km) equiangular grid. This model is based on terrestrial, altimetric and airborne gravity data.

- An average model of the Earth's gravity field, the EIGEN-GRGS.RL04.MEAN-FIELD (Lemoine et al., 2019), hereafter referred as EIGEN, computed from the RL04 GRACE+SLR monthly time series and GOCE data.

Along CalNaGeo track, the comparison with XGM2019e and EGM08 gradients shows no significant differences (resp. Fig.

630 E1b and E1c). On the contrary, the comparison with the EIGEN model shows a residual southeast/northwest gradient of about 1.8 cm/km (Figure E1d). In our process, we thus select the XGM2019e model to account for geoid gradients.

Table E 1. Geoïd height difference between the altimeter crossover and Noumea tide-gauge site

	Geoïd height difference
XGM 2019e (Zingerle et al., 2020)	-52.4 cm
EGM 2008 (Pavlis et al., 2012)	- 54.9 cm
EIGEN (Lemoine et al., 2019)	- 27.0 cm
Our study ($\Delta datum_{TG \rightarrow PG}$)	-56.2 cm
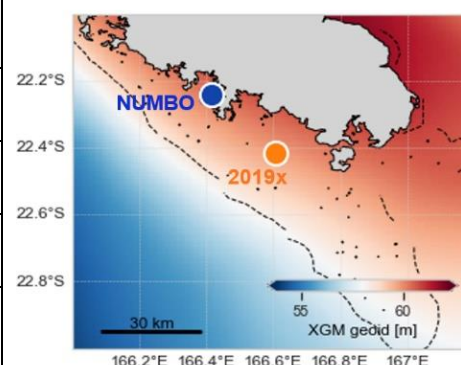
635
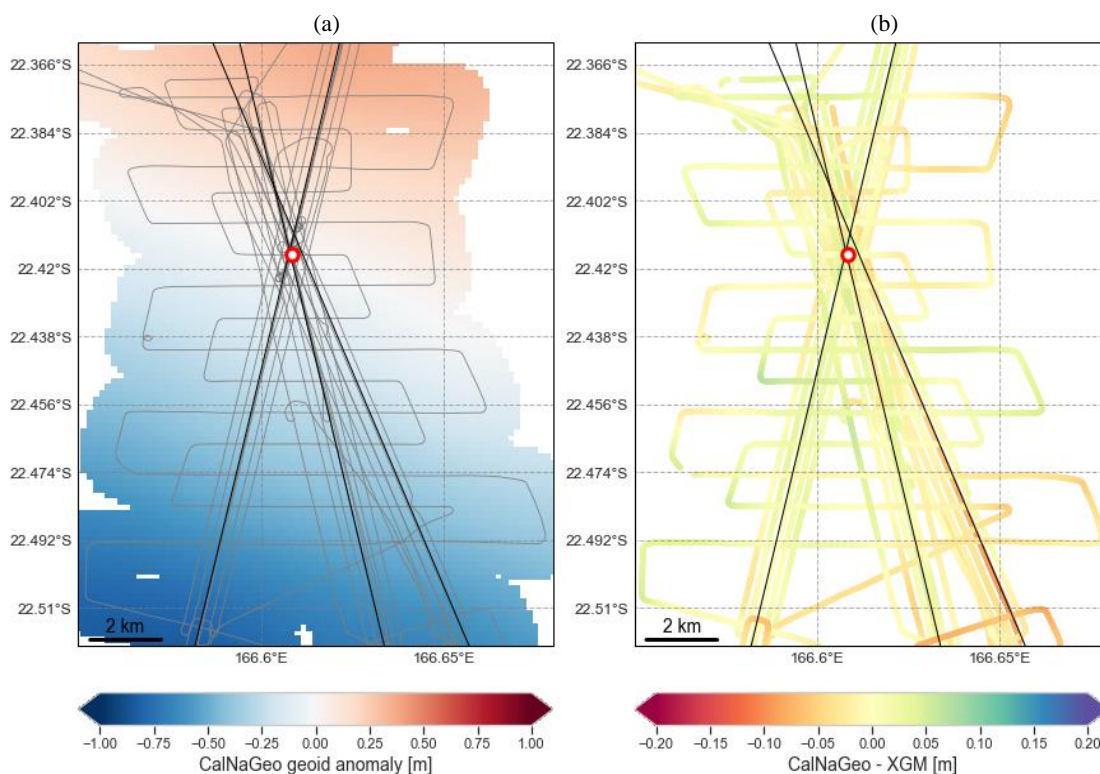
640

645
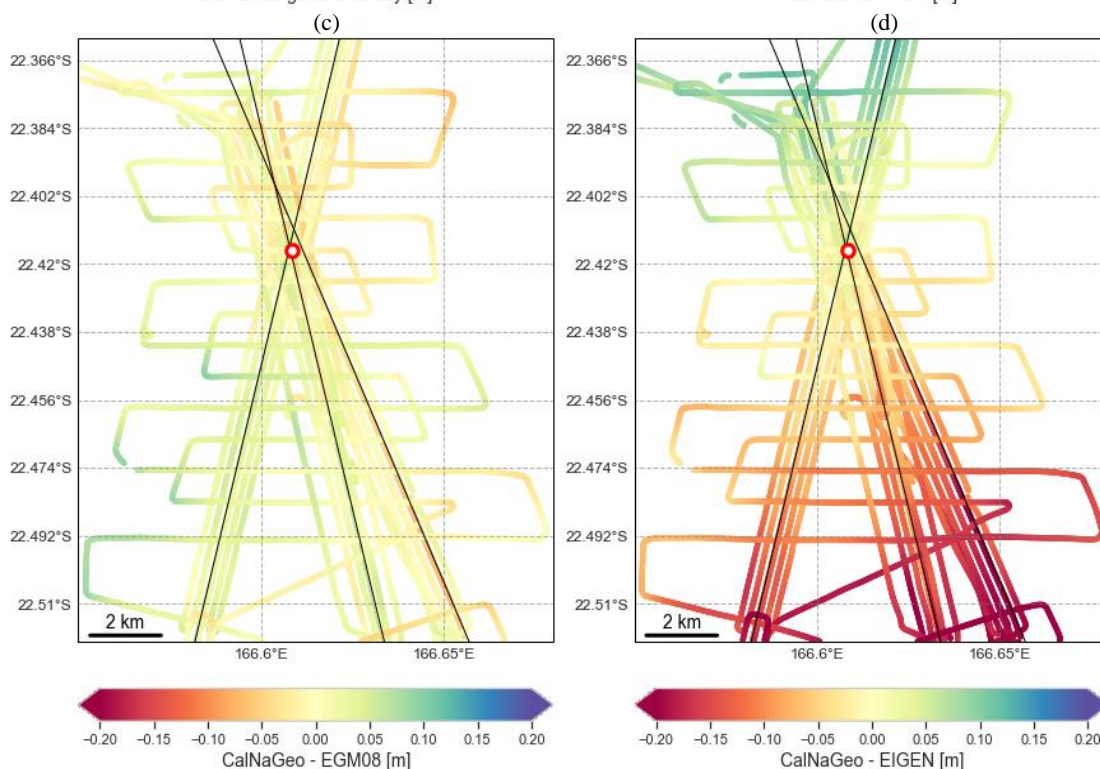
650

655

660

Figure E 1. Comparison of global gravity field models with CalNaGeo measurements. / (a) Mean sea surface anomalies from CalNaGeo measurements during the GEOCEAN-NC cruise, expressed with respect to the altimeter comparison point (red dot on the map) / (b) Difference between CalNaGeo and the XGM2019e model with respect to the comparison point. / (c) Difference between CalNaGeo and the EGM08 model with respect to the comparison point. / (d) Difference between CalNaGeo and the EIGEN model with respect to the comparison point.

Appendix F – Assessment of altimetry data quality in the lagoon

The retracking process allow to determine the range by fitting a theorical model on the radar echo recorded by the altimeter. The Mean Quadratic Error (MQE) parameter give an idea of the retracking process: the closer the MQE is to zero, the better the chosen model reproduce the measured waveform. So far, altimetry products do not give any indication of a valid on invalid 665 MQE value. To get an idea of the "threshold" value of the MQE parameter that could discriminate valid or invalid ocean waveforms, we conducted an analysis on two Jason 3 and two Sentinel-3a tracks. For all cycles between 2016 and 2019, we extract along track 20Hz MQE parameter and compare them to the coastline distance.

670

675

680
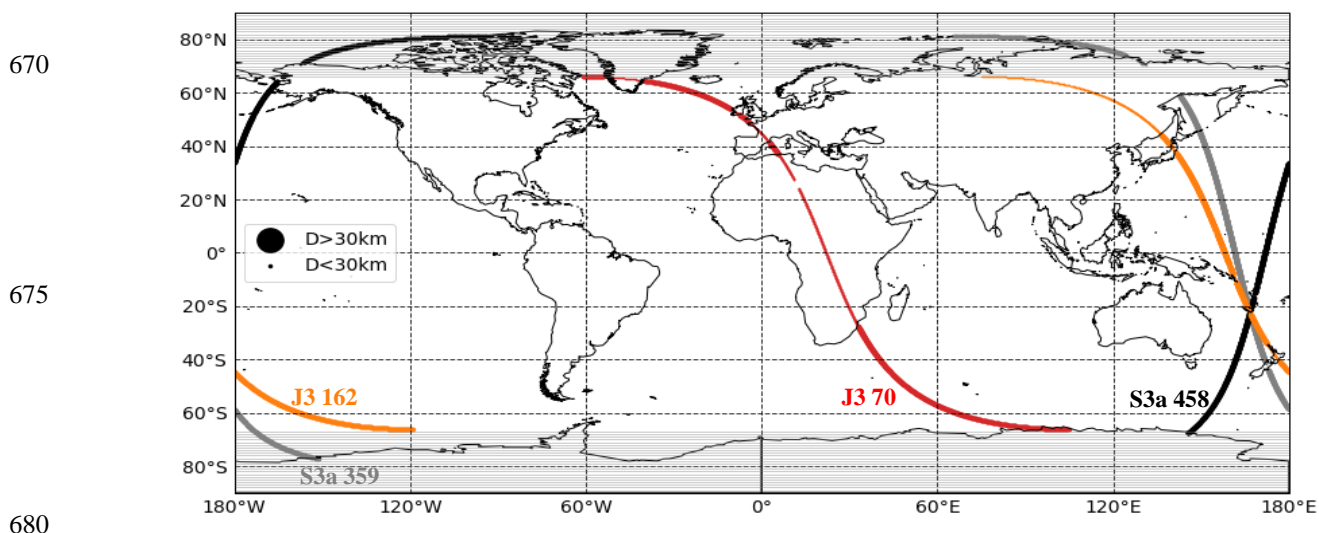
Figure F 1. Distance to nearest coastline from the along-track point of the 2 Jason and 2 Sentinel tracks used to analyse the MQE parameter. The big dots represent along-track points distant from more than 30km to the nearest coastline, and the small dots are point located on lands or less than 30km to the coastline. Note that to have a consistent comparison between both missions, Sentinel points located in polar areas (between -90°/-66° and 90°/66°) are not considered in the computation.
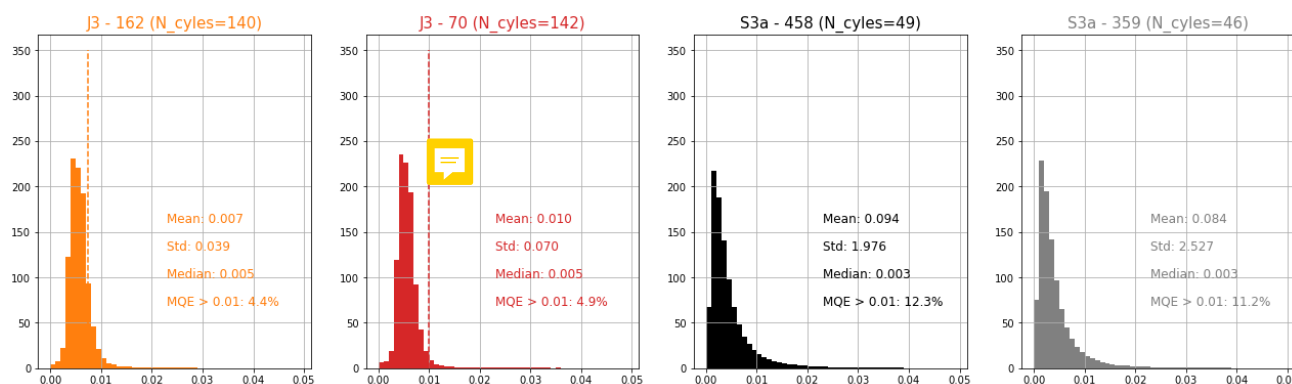
Figure F 2. Statistics on the MQE values of points located more than 30km from the coast (considered as oceanic points).
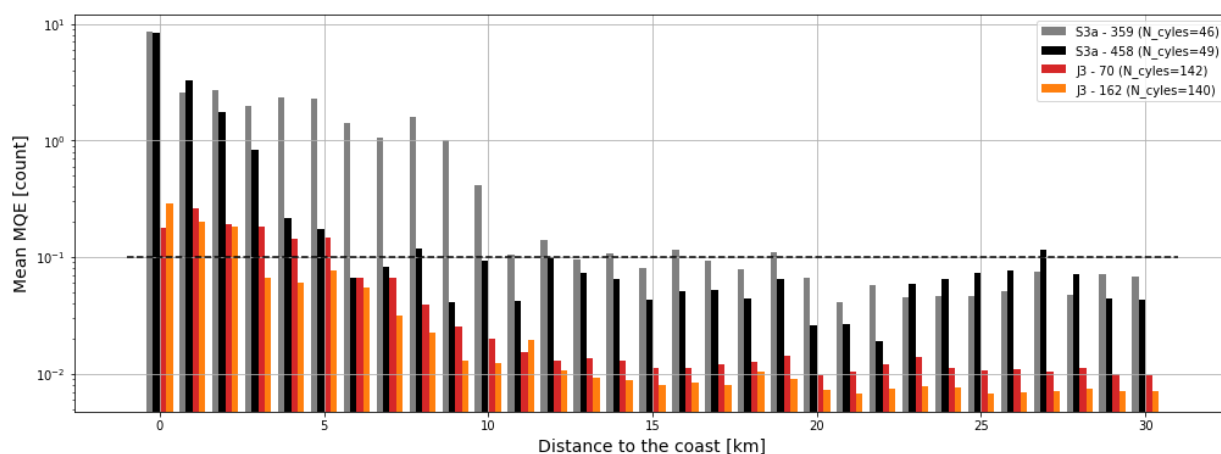
Figure F 3. Mean values of MQE parameter function of the distance to the coast.

685

For Jason 3, our analysis shows that in the open ocean (*i.e.* distance to the coast > 30 km), the mean MQE parameter is less than or equal to 0.01 (Figure F2, red and orange). Along the Sentinel-3a tracks, this mean MQE value is more variable with a standard deviation of 2/2.5 (compared to 0.04/0.07 for Jason). However, the median is well below 0.01, suggesting that extreme values influence the estimate of the mean (Figure F2, grey and black). Approaching the coast, the MQE parameter

690 increases significantly (Figure F3). In the 10/15 km range, the mean MQE tends towards 0.01 for Jason, but tends 0.1 for Sentinel (Figure F3). We could therefore consider that MQE values greater than 0.01 could indicate an improper retracking and therefore potentially erroneous water depths. These preliminary results are strongly influenced by the tracks geometry, and a global analysis of all satellite passes would help to determine a more realistic threshold value for each mission.

695 However, to analyse our dataset, we considered that a MQE value above 0,01 may indicate a non-oceanic radar signal for both Jason and Sentinel missions. Figure F4 shows the 20Hz along-track MQE parameter for the three tracks over the year 2019. There is about 3 times more Jason than Sentinel data, because of the difference in revisit period (respectively 9.9 and 27 days for Jason 3 and Sentinel satellites). We can note that for each track, the MQE parameter is higher and more variable at the coral reef overfly (black dotted line). Closer to the coast, the MQE parameter in the crossover area (black box) is mostly

700 below 0.01, indicating that the waveforms retracking using the open ocean model is suitable for most passes. As the retracking allows to determine the altimeter range, and thus to compute the altimeter Sea Surface Height, this result supports the idea that SSH altimetry data in our comparison area are reliable.
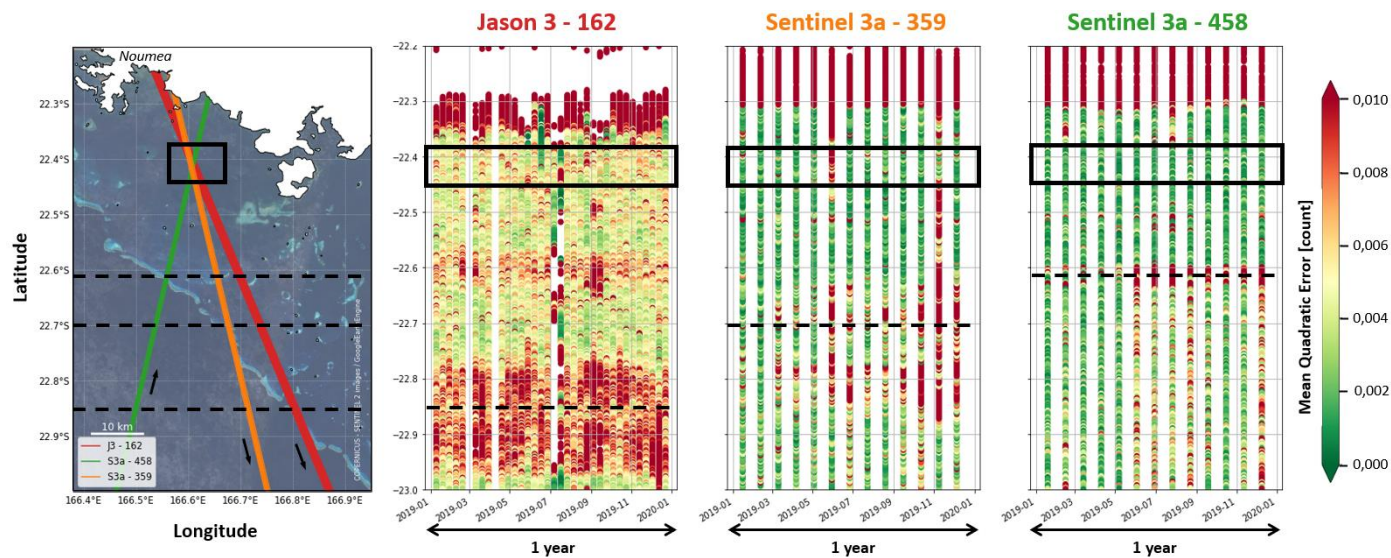
Figure F 4. Along track Mean Quadratic Error (MQE) parameter for the 3 satellites passes that crosses in the lagoon during year 2019. The grey area represents the crossing area, and the black dotted lines the open-ocean/lagoon interface for each track.